

# Large-scale shaking table tests of a six-story floor-by-floor assembled CFS frame-framing shear wall structure

Fu-Wei Wu<sup>a</sup>, Yuan-Qi Li<sup>a,b,\*</sup>

<sup>a</sup> Department of Structural Engineering, Tongji University, Shanghai 200092, China

<sup>b</sup> State Key Laboratory of Disaster Reduction in Civil Engineering, Shanghai 200092, China



## ARTICLE INFO

### Keywords:

Cold-formed steel frame  
Cold-formed steel framing shear wall  
Multi-story building  
Floor-by-floor assembling  
Shake table test  
Seismic performance

## ABSTRACT

To study the seismic performance of a proposed multi-story floor-by-floor assembled structure using cold-formed steel (CFS) frame with square columns and double-channel beams connected by novel joints, and CFS framing walls as shear walls, shake table tests were conducted on a 2:3 scaled six-story CFS frame-framing shear wall structure (CFSF-FSWS) using bidirectional seismic inputs. A prefabricated concrete floor slab was proposed utilizing the channel section beams as the molds during prefabricating processes. The CFS framing shear walls were designed with various configurations researched before: framed or trussed skeleton, single or double side sheathing, flat or corrugated steel sheathing sheet. The observed damages, dynamic properties, seismic responses and failure mechanisms of the CFSF-FSWS under different peak ground accelerations (PGAs) were analyzed. The CFS frame carried gravity load, and the horizontal earthquakes were mainly resisted by CFS framing shear walls. The results indicated a good deformation capacity and seismic performance of the CFSF-FSWS building. The damping ratio of the test model gradually increased with the accumulation of damage, varying between 3.30% ~6.95%. After all seismic loading, the CFS frame remained intact and the damages were concentrated on the CFS framing shear walls, achieving the design objective of “separated gravity and lateral resisting systems”.

## 1. Introduction

Cold-formed steel (CFS) framing wall structures have been widely applied in low-rise buildings. Recently, efforts have been made to extend the applications to multi-story and even mid-rise buildings. In higher CFS structures, besides the inter-story shear forces and overturning moments, the greater gravity loads challenge the bearing capacity and efficiency of the vertical load-bearing system. In addition, building industrialization promotes the CFS with the advantages of cold-formed manufacturing and efficient cross-sections. These properties place high demands on assembling convenience and load-bearing capacity. Therefore, there is an urgent need for high-performance CFS framing shear wall, efficient structural system and advanced design concept to meet the requirements of higher CFS structures.

In the wall component level, high-performance CFS walls with innovative configurations have been proposed to achieving higher bearing and deformation capacities. Zhang et al. [1–3] found that with proper slits on the corrugated sheathing, the CFS walls showed an improved high ductility without significant reduction in shear strength and stiffness. Yu et al. [4] further developed energy dissipation X-

bracings in CFS walls to improve the ductility. In addition to the sheathing, improvements on the skeleton configuration have also been investigated. Shi et al. [5] studied the seismic behavior of a CFS wall with diagonal braces and it was found that the lateral resistance increased slightly owing to the buckling of transverse braces. Li et al. [6,7] investigated novel CFS trussed shear walls. The results showed that the additional truss braces significantly improved the strength, stiffness and energy dissipation performances of the walls. As a new wall configuration which sandwiching the thin steel sheet between boundary members, the mid-ply CFS shear walls were tested and proved that the configurations showed a higher shear strength and good ductility [8–10]. Moreover, the measures to improve the performance of CFS walls included compositions with other materials, such as spraying the sheathing with lightweight mortar [11] or lightweight expanded polystyrene mortar [12], infilling the wall with FGD gypsum [13,14], etc.

As for the CFS structural systems, in addition to adopting high-performance walls, researchers have also worked to combine walls with other structural systems. By referring to the steel plate shear wall system [15,16], the combination of CFS walls and frame system could maximize the advantages of both. Ye et al. [17,18] used the concrete-

\* Corresponding author.

E-mail addresses: [wufuwei@tongji.edu.cn](mailto:wufuwei@tongji.edu.cn) (F.-W. Wu), [liyq@tongji.edu.cn](mailto:liyq@tongji.edu.cn) (Y.-Q. Li).

filled rectangular steel tube (CFRST) columns as the chord studs of CFS walls. Although the measures were more like a kind of wall reinforcement, the CFRST columns and I-shaped joist formed an actual frame system. The two- and three-story specimens exhibited good energy-dissipating capacity after wall yielding. Tian et al. [19] combined steel frame with infilled CFS trussed shear wall studied in reference [6] and proposed the SFIW structural system. The test results showed that the steel frame and infilled CFS walls resisted lateral forces together and exhibited good hysteretic performance. Sharafi et al. [20,21] replaced some CFS chord studs with hot-rolled SHS frame. The additional SHS frame acted as a lateral load-resisting component and significantly improved the pinching hysteretic behaviour of the hybrid wall panel. However, most of the studies on frame-CFS wall systems only conducted component-level experiments.

Shaking table test is the most direct way to verify the seismic performance of components and structures at the system level under actual earthquakes. In recent years, researches with shaking table tests of CFS structures mainly focused on low-rise buildings. Early studies involved single-story [22] and two-story CFS structures [23]. Three full-scale shaking table models of two-story CFS buildings tested by Li et al. [24] were the early experimental study to investigate the system-level seismic performance of CFS structures. The lateral force resisting systems consisted of OSB-sheathed and corrugated sheet-sheathed walls. The results showed that the low-rise CFS buildings could resist high-intensity earthquakes. Peterman et al. [25–27] conducted the shake table tests on a full-scale two-story CFS structure with OSB-sheathed walls. The structure model was tested and compared in two stages: without or with nonstructural components. The results demonstrated that the structure exhibited excellent performance and the nonstructural components reduced the forces in the shear-wall chord studs. Fiorino et al. [28,29] carried out shake table tests on a full-scale two-story sheathing-braced CFS building and then two 1:3 scaled three-story CFS building with strap-braced walls. The tests revealed the seismic performance, the effect of finishing material on structural stiffness and the in-plane behaviors of different floor types. Zhao et al. [30] presented the shake table test results of a full-scale two-story CFS structure with corrugated steel sheathed shear walls. The test model exhibited good seismic performance under extremely rare earthquake loading conditions. However, relatively fewer shaking table tests have been conducted on multi-story CFS structures. Wang et al. [31–33] conducted earthquake and post-earthquake fire testing to evaluate the performance of full-scale six-story prefabricated CFS shear wall structure buildings. The structure adopted traditional gypsum-steel-sheathed CFS walls. The seismic responses, failure phenomenon and design implications were investigated. Ye et al. [34,35] conducted shaking table tests on two 1:2 scaled five-story CFS buildings. The effects of normal and reinforced beam-column joints (as proposed in reference [17,18]) on seismic behavior and damages were investigated. Zhou et al. [36] conducted the shake table tests on a full-scale six-story CFS-steel plate shear wall structure using bidirectional seismic inputs. The lateral resisting system consisted of a kind of mid-ply CFS shear walls previously investigated [10]. The effects of multi-story system and nonstructural members were discussed. In general, current shaking table tests on low-rise and multi-story CFS structures always used lightweight floors due to test limitations or design intents, resulting in a small total mass. And few test on frame-CFS wall system was reported.

Although the above-mentioned studies have conducted vast theoretical and experimental research on CFS structures including some shaking table tests, the understandings of seismic performance of multi-story CFS structures were still inadequate, especially with regard to dual structure system combining CFS walls and steel frame. For taller CFS structures, the structural members need to bear greater vertical (gravity) loads and horizontal loads (especially the seismic loads). However, the load bearing efficiency of thin-walled members under increasing vertical loads is generally not high due to the accompanying local instability or distortional buckling. Moreover, traditional CFS walls with sheathing of

brittle material (OSB boards, gypsum boards, etc.) usually have difficulty in meeting the high deformation requirements of multi-story structures. While the CFS frame system consist of thick-wall CFS members generally owns favorable vertical load bearing efficiency. Therefore, based on the previously studied high-performance CFS wall tests [6] and wall-frame tests [19], a multi-story floor-by-floor assembled CFSF-FSWS system was proposed and tested through shaking table tests in this paper. The structural system was designed with the concept of “separated gravity and lateral resisting systems”, leveraging the strengths of both systems to achieve optimal performance. The hinged CFS frame system for gravity load had favorable lateral deformation capacity and vertical bearing capacity. The high-performance CFS framing shear wall system became the main lateral-force resisting system. Many innovative construction measures have been developed and practiced to ensure the floor-by-floor assembly properties of the structural system and the reliability of the wall-frame connections. Finally, a shaking table test program on the 2:3 scaled six-story CFSF-FSWS model was conducted to verify the structural feasibility, observe whether the system achieved the expected damage phenomenon that “wall damaged while frame kept intact” and assess the seismic performance under bidirectional earthquakes. The dynamic properties, seismic responses and failure mechanisms of the CFSF-FSWS test model under different PGAs were obtained and analyzed.

## 2. CFSF-FSWS system

### 2.1. Composition of the CFSF-FSWS system

The main structural components of the CFSF-FSWS system included CFS square columns, CFS double-channel beams, floor-by-floor assembled joints, CFS framing shear walls and prefabricated concrete floor slabs, as shown in Fig. 1. In order to realize the architectural function, partition walls were usually arranged in the CFSF-FSWS buildings, which were considered as non-structural components and carried no load. The CFS square columns, CFS double-channel beams and floor-by-floor assembled joints together formed the CFS frame system, which was subjected to gravity load. The CFS frame system was designed with weak column-joint connections and hinged beam-joint connections, and therefore with low inter-story stiffness and favorable deformation capacity. The CFS framing shear walls with higher stiffness carried the major lateral loads and became the main lateral force-resisting system. Therefore, the CFSF-FSWS system achieved the “separated gravity and lateral resisting systems” design concept. Compared to thin-walled components, the CFS frame system carried vertical loads with high efficiency. Meanwhile, the design of hinged frame increased assembling efficiency and demanded low plastic deformation capacity of the components. The CFS framing shear wall system was then able to maximize the lateral resistance without gravity load. The advantages of both systems were fully exploited. It was noted that in the actual shaking table tests, to facilitate the installation of the test model with the shaking table, the split-type bases for bottom columns and walls were adopted, which were made of steel plates and stiffening ribs with sufficient thickness to achieve the rigid foundation.

### 2.2. Floor-by-floor assembled joint

A new floor-by-floor assembled joint was proposed to accommodate the installation of the CFS frame system in CFSF-FSWS based on the similar joint configurations [37]. The main configurations of the joint, including the connected column and beam components, are shown in Fig. 2. The frame column adopted CFS square steel tube with end plates welded at both ends. The column end plates were connected to the joint end plates by twelve M16 high strength bolts. The frame beam adopted CFS double-channel beam, which joining two CFS channels to form an H-section beam. The two CFS channels were connected by M16 bolts through the bolt holes in the webs. The CFS double-channel beam

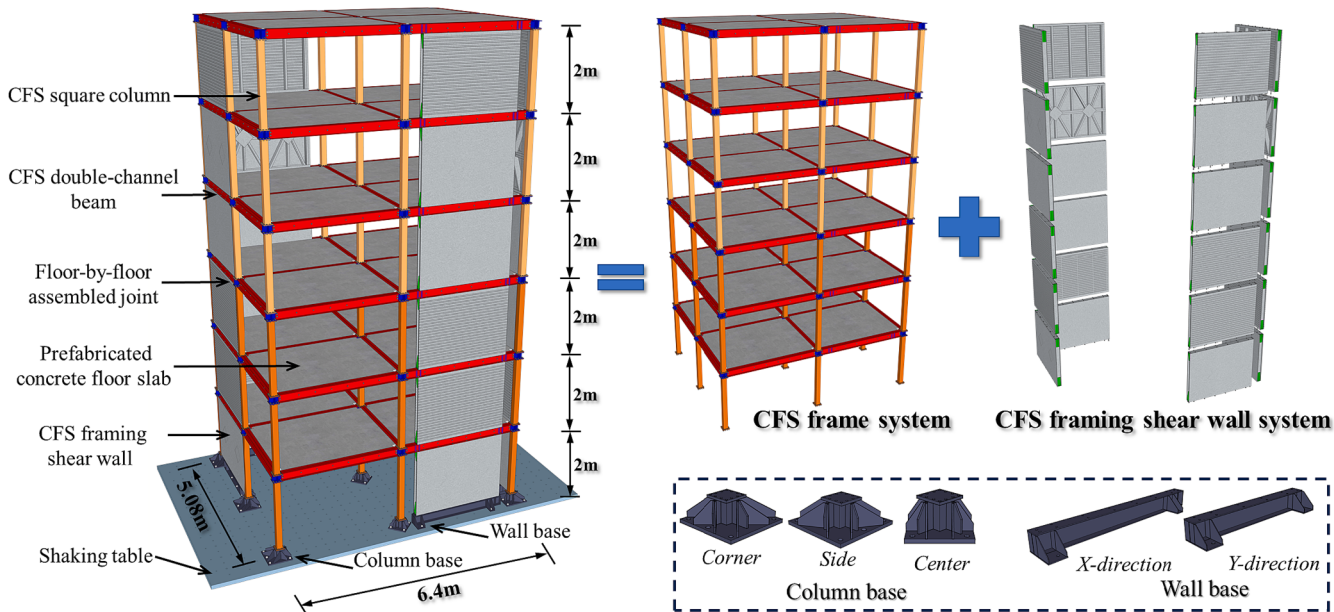


Fig. 1. CFSF-FSWS system model and structural composition.

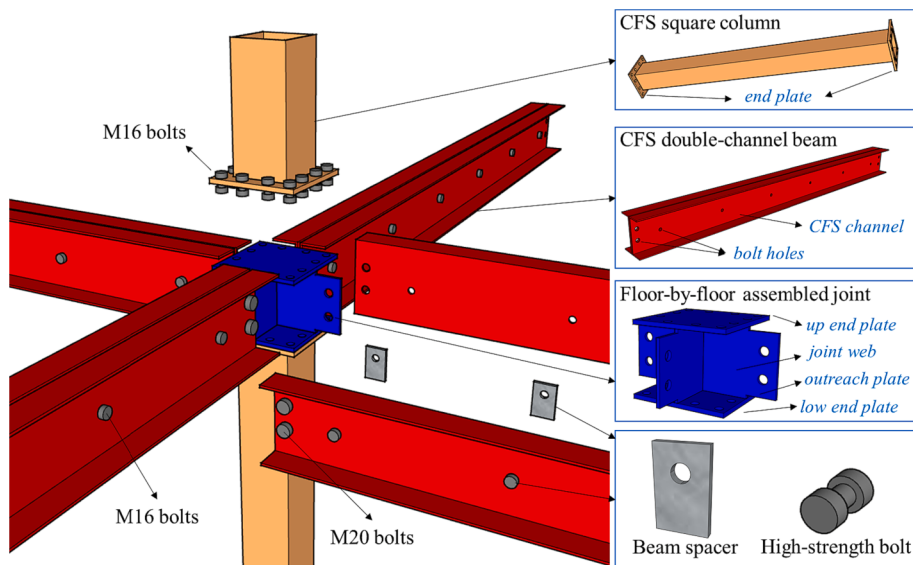


Fig. 2. Floor-by-floor assembled joint.

clamped the outreach plate of the joint web and was connected to the outreach plate of the joint web by two M20 high strength bolts. The flanges of the beam were not connected to the joint, thus forming a typical hinged beam-end connection which transmitted shear force but almost no bending moment. The space between the webs of the two CFS channels were filled by spacers with the same thickness as the outreach plates. The joint web was a cross-type section. Since the cross-section area of the joint web was concentrated in the center, it had a lower moment of inertia (cross section stiffness) compared with the tubular section with the same area. Therefore, the whole joint was weakly semi-rigid at the column-end connection and hinged at the beam-end connection. This made the CFS frame system carried very limited lateral loads in the earthquakes. The CFS framing shear wall system became the predominant lateral force resisting system. Moreover, the weak stiffness of the joint subsequently resulted in the good elastic inter-story deformation capacity, which ensured the safety of the CFS frame system. These characteristics were designed to realize the proposed

“separated gravity and lateral resisting systems” design concept. In the installation processes, the 1st story frame columns were installed on the bases first, then the joints were installed on the column. After that, the beams were installed on the joints (actually together with the concrete slab as a whole). This step was followed by the installation of the 2nd story columns, and so on, thus realizing the so-called floor-by-floor assembly with high assembling convenience.

### 2.3. Prefabricated concrete floor slab

A novel type of prefabricated concrete floor slab was proposed, which fully utilized the characteristics of double-channel beams. The detailed manufacturing processes and configurations are shown in Fig. 3. The concrete slab was fabricated surrounding by four CFS channel beams. A proper number ( $4 \times 4$ ) of steel brackets were welded to the beams and embedded into the concrete to carry the concrete slab. Two shear resistant bolts were welded on each of the steel bracket for

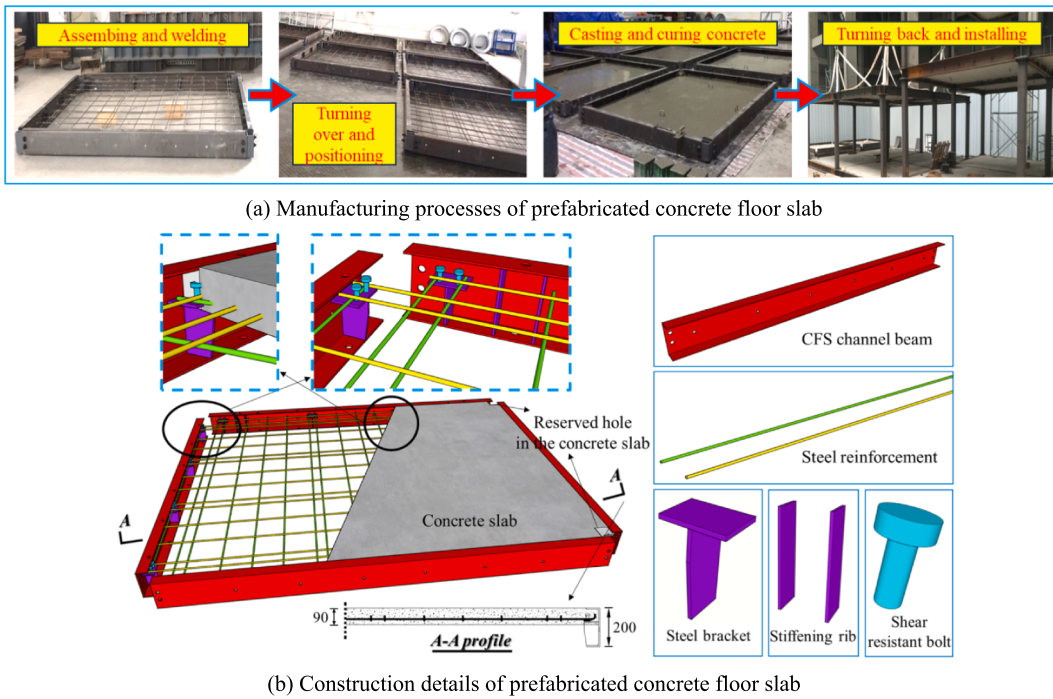


**Fig. 3.** Prefabricated concrete floor slab.

securing the concrete slab and transferring possible in-plane shear forces. The X- and Y-directional reinforcement bars were laid out, with the ends of the bars welded to the steel brackets. The location of the reinforcement bars was in the lower part of the concrete slab, forming a conventional reinforced concrete slab in combination with the concrete. Bolt holes in the concrete slab were pre-set at the locations where bolt holes were set on the beam flange (for the purpose of connecting the CFS framing shear walls). At the same time, stiffening ribs were welded at the connecting location of the shear-wall hold-down bolts. The stiffening ribs ensured the transfer of large axial loads from the hold-downs. In the manufacturing processes (Fig. 3a), the four CFS channel beams were firstly assembled by temporary fixtures and placed in positive direction. After welding the steel reinforcement, the assembled members were turned over in reverse direction and positioned on the bottom formwork. The channel beams around the four sides were then used as lateral concrete molds. Finally, the concrete was poured, controlling the concrete depth to 90 mm, which was less than the beam height (200 mm). When installing, the floor slabs were turned back in positive direction and connected by bolts after removing the temporary fixtures. In the structure, the concrete slab was within the height of the channel beams and located in the upper position, solving the problem of floor slab occupying the story clear height. The way of pouring and molding the channel beams and concrete slab in one piece also enabled the proposed prefabricated concrete floor slab to have favorable floor-by-floor assembling characteristics.

#### 2.4. CFS framing shear wall

The CFS framing shear walls adopted the high-performance steel-sheathed CFS walls studied in the previous researches [6,7,19]. The built-up chord studs and hold-downs met the requirements of multi-story CFS structures. The detailed configurations of the CFS framing walls were described in [Section 3.3](#).

#### 2.5. Connection of wall to frame

The connections between the CFS wall system and the CFS frame system were a vital part in the structural design. The connections should

ensure the load transfer between the two system so as to achieve the cooperative working. The all-bolted connections between the CFS walls and the CFS frame were divided into two categories: hold-down connections and CFS wall track connections. The schematic diagram and key details of the hold-down-to-frame bolted connection are shown in [Fig. 4](#). Considering the consistency of the lateral force resisting in both horizontal directions, CFS shear walls of the same width were set. For the larger span in X-direction, the column-wall space of 330 mm width naturally existed. This kind of non-full-span arrangement of shear walls made more flexibility in design. The hold-downs of the X-directional walls were connected to the double-channel beam flange with two M20 bolts. The vertical forces generated by the overturning moments of the wall were transferred from chord stud to hold-down to frame beam and finally to the hold-down of the adjacent wall. The beam here mainly acted the role of vertical force transmission for the hold-downs above and below. The open-section beams were strengthened with stiffening ribs at the force-transferring positions. Longer bolts were used because the inward M20 bolts needed to pass through the concrete floor slab. For the hold-down connection of the Y-directional wall, the hold-down was located exactly on the column end plate. The connections of the hold-down to the CFS frame here shared the two M16 bolts belonging to the connections between column end plate and joint end plate. Moreover, the hold-down was in a closed space due to the close fit of the Y-directional wall and the frame column. The bolted connection here adopted one-side bolts.

The schematic diagram and key details of the track-frame bolted connection are shown in [Fig. 5](#). The connections of the X- and Y-directional walls were the same, so the connection illustration of the X-directional wall was used here as an example. The track-frame bolts mainly transferred the shear forces from the wall to the beam. Two rows of six M16 bolts were arranged for each track. Bolt holes were pre-set at the corresponding locations of the tracks' webs and beams' flanges. Similarly, longer bolts were used because the inward M16 bolts of the bottom track needed to pass through the channel beam with concrete floor slab. In the installation processes, the bolted connections of the CFS framing shear walls to the CFS frame should be done after the assembly of the CFS frame (including the floor slab), thus ensuring that the gravity loads were borne by the CFS frame system.

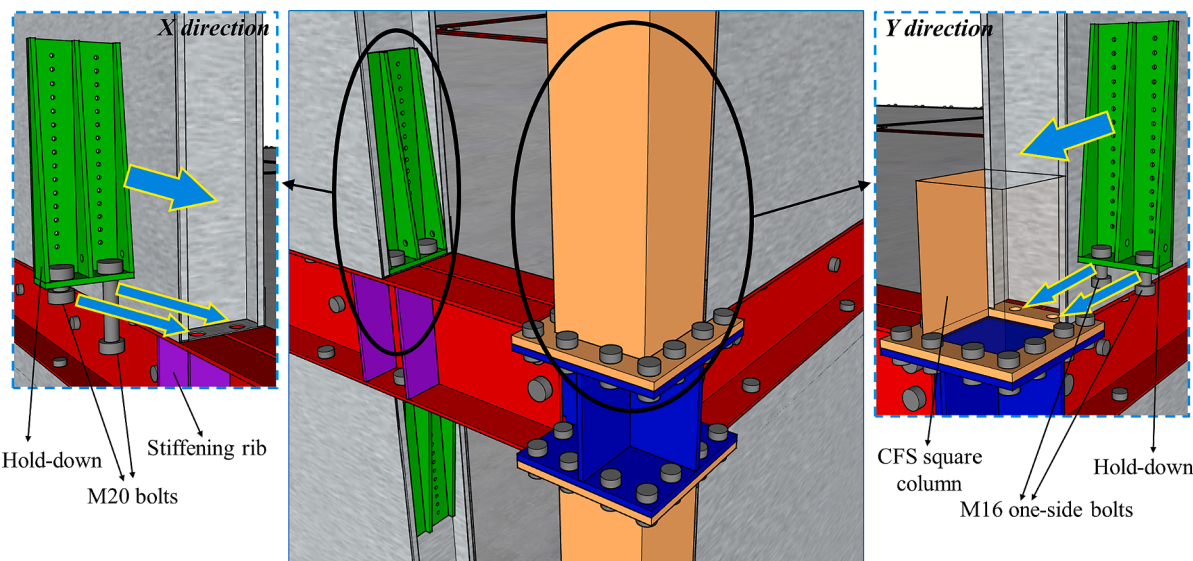


Fig. 4. Hold-down-to-frame bolted connection.

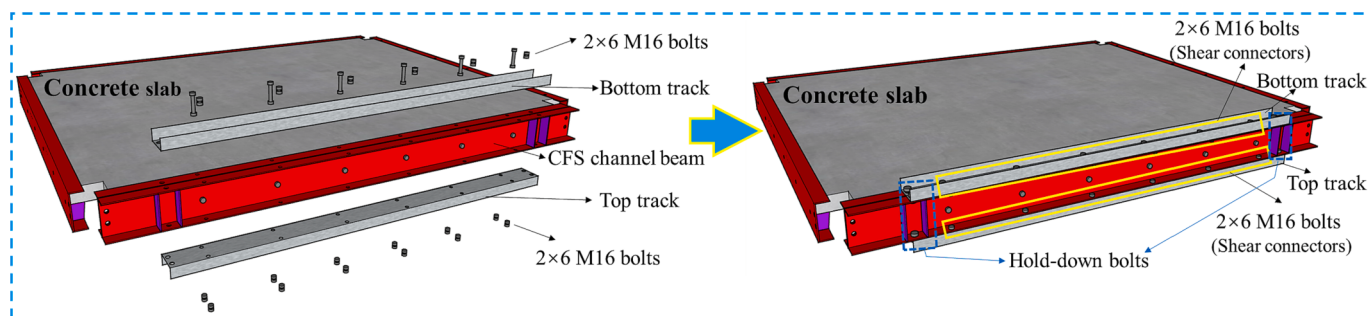


Fig. 5. Track-frame bolted connection.

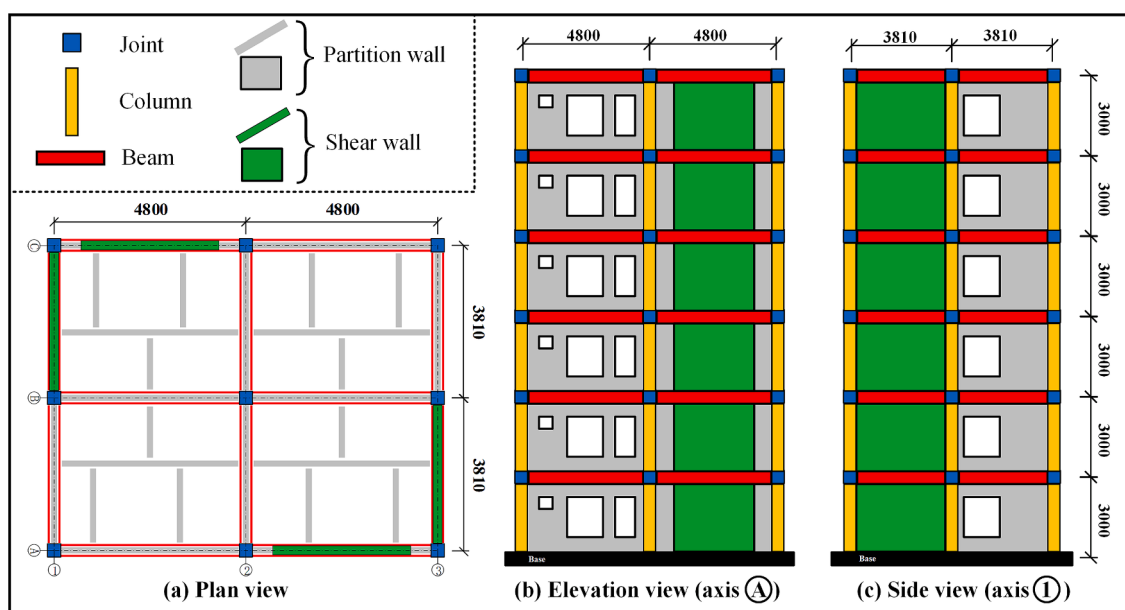


Fig. 6. Dimensions of the prototype building.

### 3. Shaking table test design

#### 3.1. Prototype building

The prototype building was a residential building designed in a high seismic intensity region of China with the seismic precautionary intensity level of 8. According to the Chinese Code for the Seismic Design of Buildings (GB50011-2010) [38], the seismic design of the prototype building was based on the second earthquake group, the IV class site condition, and a design spectral acceleration of 0.2 g (i.e., Life Safety, for earthquakes having 10% probability of exceedance in 50 years). The prototype building is shown in Fig. 6, with a story height of 3 m and a total of 6 stories. The prototype building was constructed with CFSF-FSWS structural system and followed all the technologies described in Section 2.

#### 3.2. Similarity relationship

The shaking table tests were conducted on a large shaking table equipment with the plane size of 6.0 m × 10.0 m (combining two sub-tables). The total mass of the test model was limited to 140 ton. The maximum horizontal acceleration value was ± 1.5 g. The overturning moment of each of the two sub-table was 400 ton-m. Due to the limitation of the maximum height of the laboratory and the load capacity of the shaking table, The prototype building should be scaled. By reasonably designing the similarity relationships between the scaled test model and the prototype building, the seismic performance and responses of the CFSF-FSWS could be well reflected [39]. Considering the mechanical properties of the prototype building, the laboratory height, and the dimensions and capacity of the shaking table, three basic scale factors of the test model were determined as follow: the length scale factor ( $S_l$ ) was 2/3; the stress scale factor ( $S_\sigma$ ) was 1.0, and the acceleration scale factor ( $S_a$ ) was 1.5. Then, based on these three basic factors, the scale factors of other physical parameters were derived according to the dimensional analysis method (i.e., Buckingham  $\pi$  theorem) [40]. The derivation processes and calculated scale factors are summarized in Table 1.

#### 3.3. Test model design and configuration

The test model was manufactured and installed in accordance with a 2:3 scaling ratio to the prototype building, as shown in Fig. 7. The scaled test model was within the limitations of the lab conditions. Moreover, the big scaling ratio 2:3 was set to utilize the shaking table loading

**Table 1**  
Derivation processes and calculated results of the scale factors.

Category	Physical parameter	Relation	Scale factor
Material property	Strain	$S_e = S_\sigma / S_E$	1.0000
	Stress	$S_\sigma$	1.0000
	Elastic modulus	$S_E = S_\sigma$	1.0000
	Poisson's ratio	$S_\nu$	1.0000
	Mass density	$S_p = S_\sigma / (S_a S_l)$	1.0000
Geometric property	Length	$S_l$	0.6667
	Area	$S_S = S_l^2$	0.4444
	Displacement	$S_d = S_l$	0.6667
	Rotation angle	$S_\theta = S_\sigma / S_E$	1.0000
Load property	Force	$S_F = S_\sigma S_l^2$	0.4444
	Linear load	$S_q = S_a S_l$	0.6667
	Area load	$S_p = S_\sigma$	1.0000
	Moment	$S_M = S_a S_l^3$	0.2963
Dynamic property	Mass	$S_m = S_a S_l^2 / S_a$	0.2963
	Stiffness	$S_k = S_a S_l$	0.6667
	Period	$S_T = S_l^{0.5} S_a^{-0.5}$	0.6667
	Frequency	$S_f = S_l^{-0.5} S_a^{0.5}$	1.5000
	Damping	$S_c = S_a S_l^{1.5} S_a^{-0.5}$	0.4444
	Velocity	$S_v = (S_l S_a)^{0.5}$	1.0000
	Acceleration	$S_a$	1.5000

capacity as much as possible, and to avoid the manufacturing difficulties, material errors and response distortions. The 2:3 scaled model could be seen as an almost full-scale model. The test model included all beams, columns, joints and lateral force resisting components (CFS framing shear walls). However, the partition walls, which were seen as the non-structural components, were ignored in the tests. As shown in the schematic diagram in Fig. 7 and the real shots in Fig. 8, the test model was a six-story structure with two spans in each of the two horizontal directions. The story height was 2 m, and the total height was 12 m. The spacing of the columns along the lateral direction (X-direction) was 3200 mm, and the spacing of the columns along the longitudinal direction (Y-direction) was 2540 mm. The widths of CFS framing shear walls were all 2400 mm.

#### 3.3.1. CFS frame system

The CFS frame system was all manufactured with Q235 steel according to Chinese Code for Design of Steel Structures [41]. The frame column adopted the CFS square tubes. For the CFS channels used in frame beams, flat steel plates were firstly cut, and then cold-formed into channel sections by bending machines. The rest of the CFS frame components (such as joints, etc.) were all cut and welded from Q235 steel plates. The 90-mm thick prefabricated floor slab adopted C35 concrete with the nominal compressive strength of 35 MPa. The reinforcement bars of 8 mm diameter and 150 mm average spacing were set in two horizontal directions. The mechanical properties of steel plates with different thicknesses were determined by tensile coupon tests. The modulus of elasticity, yield strength and tensile strength are summarized in Table 2. The schematic diagrams of the typical CFS frame components are presented in Fig. 9. Each end of the column was connected to the joint by twelve M16 bolts through end plates. And each end of the beam was connected to the joint web by two M20 bolts. The M16 and M20 bolts used in the test model were all high-strength friction-type bolts and were tightened with the preset torque values of 229 N·m and 445 N·m respectively. It was noted that the frame columns were different in cross section (□140 × 140 × 8 for 1 ~ 3 stories and □140 × 140 × 6 for 1 ~ 3 stories).

#### 3.3.2. CFS framing shear wall system

CFS framing shear walls were the main lateral force resisting components of the CFSF-FSWS. The configurations of the CFS walls included several types: single or double side sheathing, flat or corrugated steel sheathing sheets, framed-type or trussed-type skeleton. The corresponding static tests and seismic performances of the CFS walls have been previously investigated [6,7,19]. Based on the bearing capacity and stiffness characteristics of walls, the CFS walls with different configurations were arranged for each story of the test model, as listed in Table 3. The lateral resistance provided by the walls was reduced story by story, complying with the distribution of the seismic-induced inter-story shear forces. The CFS walls were all made of S350 thin-walled steel with the nominal strength of 350 MPa. The material mechanical properties were determined by tensile coupon tests as summarized in Table 2. The detailed configurations of the CFS framing shear walls are shown in Fig. 10. The skeletons were assembled with tracks (U145 × 60 × 2.0), chord studs (C140 × 50 × 11 × 1.2, C135 × 45 × 20 × 2.0), field studs (C140 × 50 × 11 × 1.2), blockings (U142 × 56 × 1.0), bracings (C140 × 50 × 11 × 1.0) and gusset plates (360 × 360 × 2.0). It was noted that the chord studs of Y-directional walls were back-to-back sections (2C140 × 50 × 12 × 1.2), while the chord studs of X-directional walls were further strengthened with a C-shape channel (C135 × 35 × 20 × 2.0), forming a three-limb built-up section. The sheathings were all 0.8 mm thick. The type of corrugated steel sheets was YX5-70.5-915/1128-0.8, consistent with the reference [6]. The skeletons were assembled using washer head self-drilling screws (4.8-mm diameter × 25-mm length). The sheathing sheets were attached on the skeletons by hex washer head self-drilling screws (5.5-mm diameter × 38-mm length). The average spacing of the sheathing-to-member screws was 150/300 (inside/outside). Since

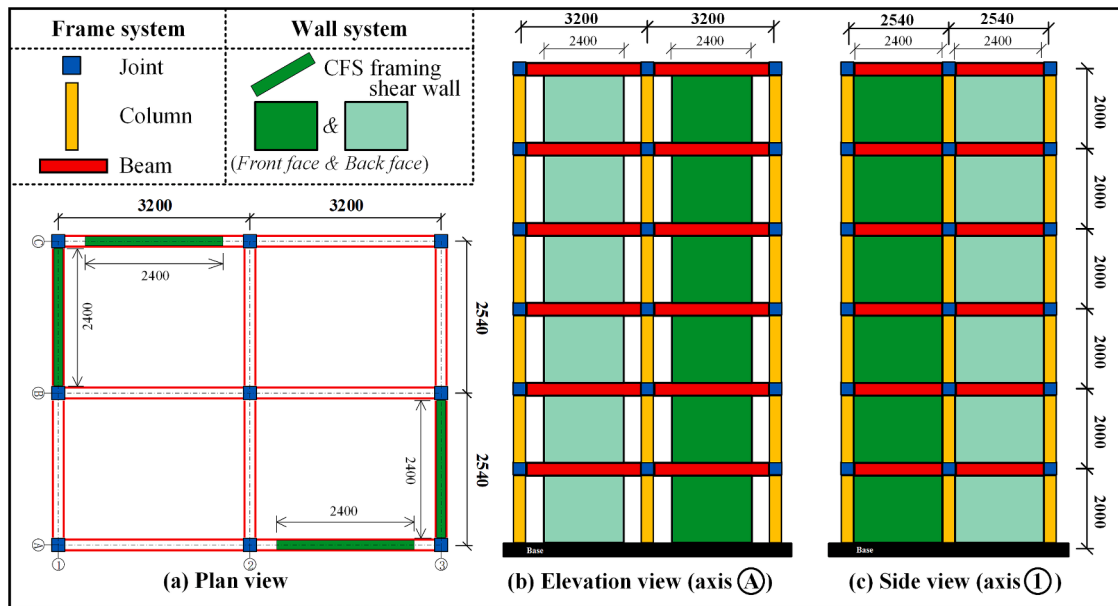


Fig. 7. Dimensions of the test model.

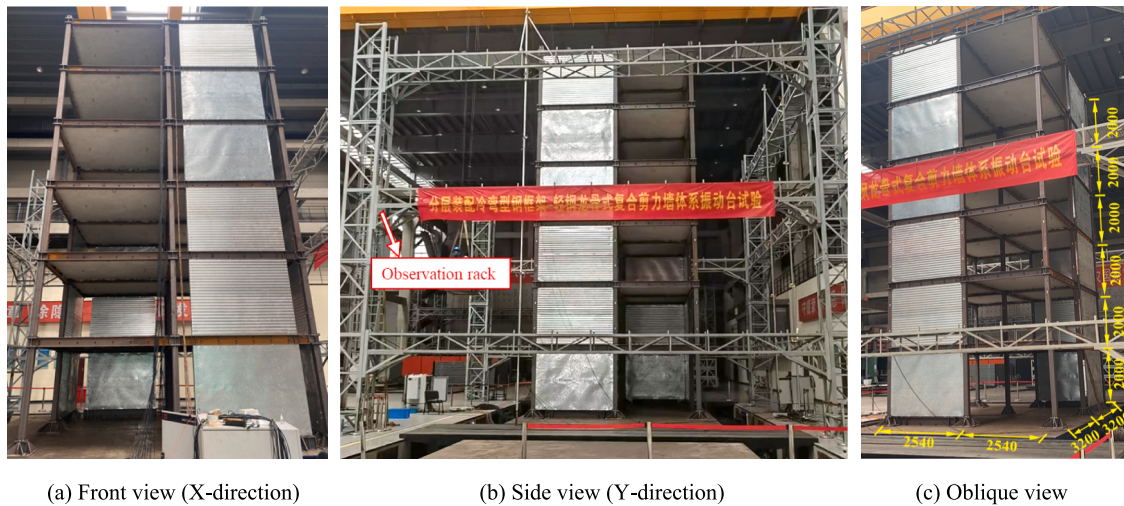


Fig. 8. Real shots of the test model.

**Table 2**  
Material properties of the steel.

Category	System	Section dimension/mm	Thickness /mm	Yield strength/MPa	Tensile strength/MPa	Elastic modulus/ $\times 10^5$ MPa
Column 1 ~ 3	Frame	□140 × 140 × 8	8	388.0	543.7	2.02
Column 4 ~ 6	Frame	□140 × 140 × 6	6	393.4	487.2	2.17
Channel beam	Frame	U140 × 70 × 6	6	378.8	522.4	2.08
Stiffening rib & Bracket	Frame	—	6	369.4	496.6	2.04
Joint web	Frame	—	8	378.4	485.0	1.94
Joint end plate	Frame	220 × 220 × 10	10	327.7	464.2	2.23
Column end plate	Frame	220 × 220 × 12	12	365.0	520.9	1.99
Sheathing	Wall	—	0.8	383.3	490.3	2.00
Bracing & Blocking	Wall	—	1.0	413.9	523.6	1.92
Stud 1	Wall	—	1.2	408.9	514.5	2.07
Track & Stud 2 & Gusset	Wall	—	2.0	358.0	504.4	1.98

the walls were subjected to large loads in multi-story structures, the hold-downs were specially designed and made with 6-mm Q235 steel (Fig. 4). Noted that the above CFS walls were designed based on the limit state design (LSD) guidelines in accordance with AISI standards [42,43]

and the specimens' configurations in references [6,19].

### 3.3.3. Loads and additional mass

According to Chinese Load Code for the Design of Building Structures

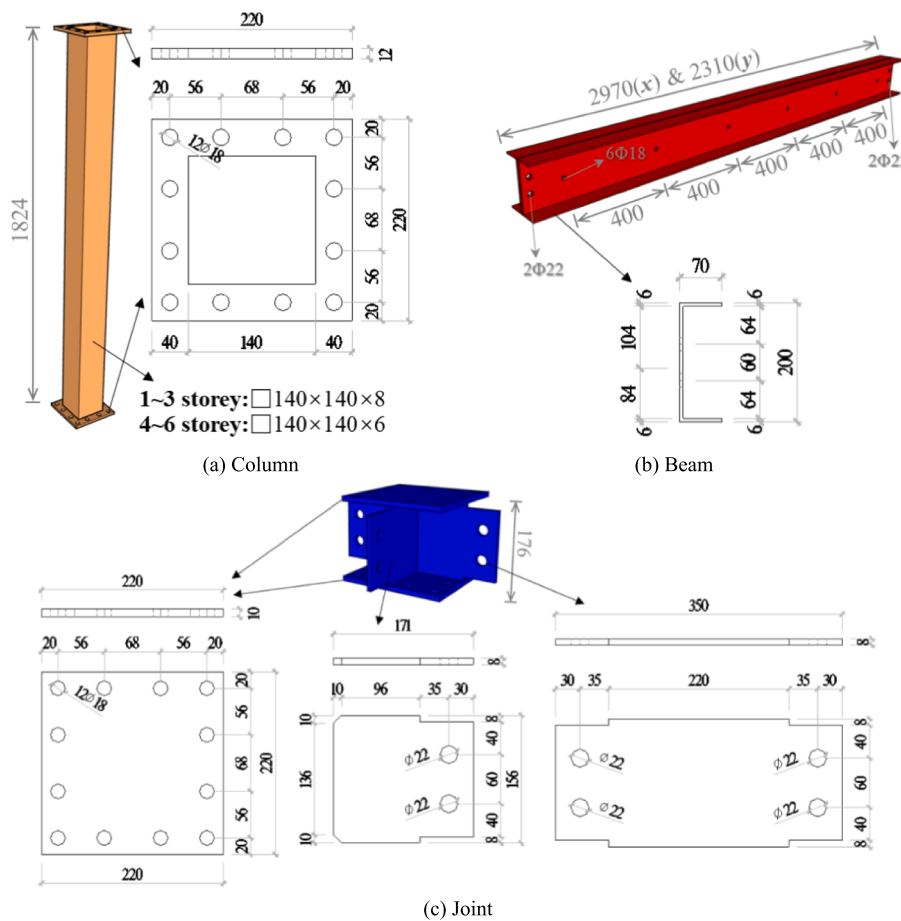


Fig. 9. Schematic diagrams of typical CFS frame components.

**Table 3**  
Arrangements of CFS framing shear walls for each story.

Story	Skeleton type	Sheathing type	Sheathing sheet 1	Sheathing sheet 2	Nominal strength of a wall (kN)
1	Trussed	Double-side	Flat	Flat	151.1
2	Framed	Double-side	Corrugated	Corrugated	126.9
3	Framed	Double-side	Flat	Corrugated	115.8
4	Framed	Double-side	Flat	Flat	104.8
5	Trussed	Single-side	Flat	-	98.8
6	Framed	Single-side	Corrugated	-	63.5

GB50009-2012 [44], the design values of dead and live loads of the prototype building were determined. The dead load was calculated based on the weights of the components and the building practice. The live load, on the other hand, was selected in the code table by the building occupation. The representative value of the total gravity load were the factored combined value of dead load and live load. The combined reduction factors were 1.0 for dead load and 0.5 for live load. For the scaled test model, the additional mass was calculated based on the representative value of the total gravity load and the mass scale factor ( $S_m = 0.2963$ ). Moreover, the remaining additional mass were determined based on the force scale factor ( $S_F = 0.4444$ ) to ensure that the test model satisfied the force similarity relationship, like the axial compression ratio of the frame columns [45]. Table 4 lists the loads of the prototype building and the additional mass of the test model. It was noted that the mass (weight) of each prefabricated concrete floor slab differed slightly from the design value due to the errors generated during concrete pouring and curing. To solve this problem, the mass of each

slab was weighed before installation, and the mass of each story was eventually the same as the design value by adjusting the number of additional mass blocks. The total mass of the test model was 65.84 ton (excluding the mass of the model bases).

### 3.4. Instrumentation

The instrumentation including acceleration sensors and displacement sensors were arranged in each story. During the test processes, the acceleration and displacement responses were collected to evaluate the dynamic properties and seismic performance of the structure. The arrangement of the sensors is shown in Fig. 11. One bidirectional accelerometer was arranged at the center of the bottom story to measure the horizontal accelerations of the shaking table (i.e., the actual input seismic accelerations). On the floor plan of the other stories (i.e., stories 1 ~ 6), two bidirectional accelerometers were arranged at the center and the upper right corner, respectively. A X-directional displacement sensor was arranged at the C-axis, and two Y-directional displacement sensors were arranged at the 1 and 2 axes of each floor plan, respectively.

In addition to instruments measuring the dynamic responses, strain gauges were arranged on CFS walls and frame columns. The arrangement of strain gauges is shown in Fig. 12. Noted that due to the limited number of channels in the acquisition equipment, strain gauges were only arranged on the columns in the second and third stories for obtaining the axial strains in the X-direction. The wall strain gauges were set to measure the strain at the positions where buckling may occur, like chord studs and bracings. The function of the strain gauges on the columns was to obtain the sectional bending moment and then the column shear force. The lateral load sharing mechanism of frame system and wall system in the test model could then be analyzed. The total shear

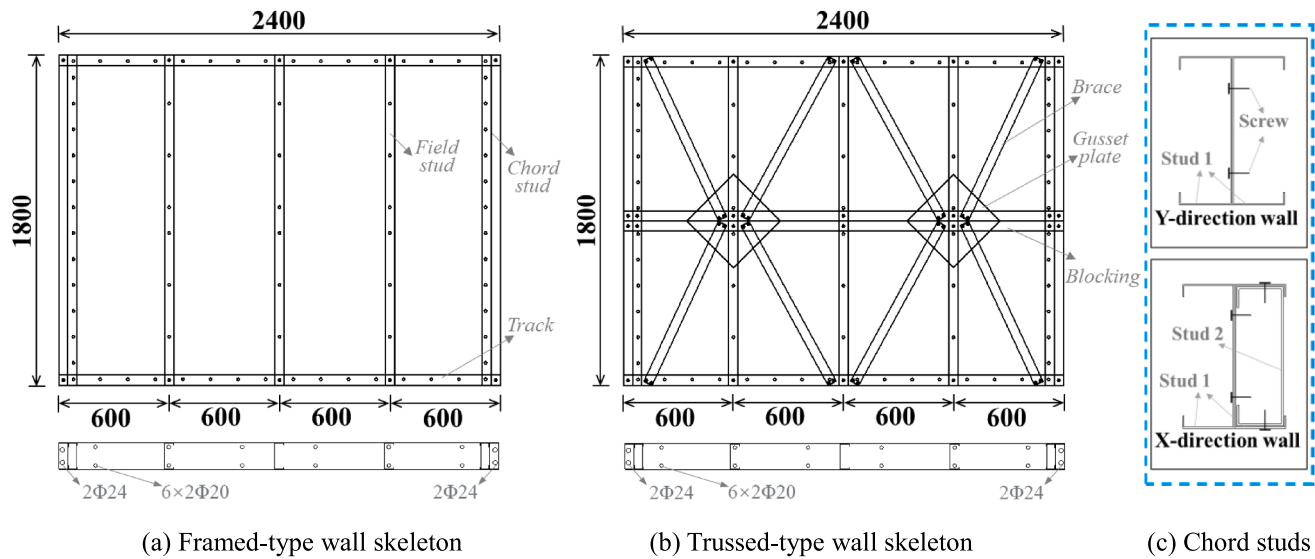


Fig. 10. Configurations of CFS framing shear walls.

**Table 4**  
Loads of prototype building and additional mass of the test model.

Location	Load type	Design value (kN/m <sup>2</sup> )	Scaled mass (ton)	Additional mass (ton)	Total mass (ton)
Floor	Dead load	2.5	7.59	3.79	11.38
	Live load	2.0			
Roof	Dead load	2.5	6.50	2.44	8.94
	Live load	0.5			

force  $Q_k$  of the  $k_{\text{th}}$  story can be obtained from Eq. (1):

$$Q_k = \sum_{i=k}^6 m_i a_i \quad (1)$$

where  $m_i$  is the mass of the  $i_{\text{th}}$  story;  $a_i$  is the acceleration of the  $i_{\text{th}}$  story.

The upper strain gauges ( $S_{c,1}$  and  $S_{c,2}$ ) and lower strain gauges ( $S_{c,3}$  and  $S_{c,4}$ ) located at 512 mm and 1312 mm of the column height,

respectively. Based on the previous numerical analysis, the 800-mm-long column segment between the strain gauges contained the contraflexure point and remained elastic during the tests. Therefore, for each frame column, the shear force can be calculated according to Eq. (2) [46]:

$$Q_{c,k} = \frac{M_u + M_l}{L} = \frac{EW(\varepsilon_{u,1} - \varepsilon_{u,2} + \varepsilon_{l,3} - \varepsilon_{l,4})}{2L} \quad (2)$$

where  $M_u$  and  $M_l$  were the upper and lower bending moments;  $\varepsilon_{u,1}$  and  $\varepsilon_{u,2}$  are the strains measured by the upper strain gauges;  $\varepsilon_{l,3}$  and  $\varepsilon_{l,4}$  were the strains measured by the lower strain gauges;  $L$  was the vertical distance between the strain gauges;  $E$  was the elastic modulus of steel; and  $W$  was the section modulus of the frame column [47].

### 3.5. Loading scheme

In accordance with the Chinese Code for Seismic Design of Buildings [38], three natural earthquakes and one artificial earthquake were selected as the seismic excitations for the shaking table tests. The three natural earthquakes included: El-Centro earthquake (May 18, 1940), Taft earthquake (July 21, 1952) and Kobe earthquake (January 17, 1995). The artificial earthquake was the Shanghai wave (i.e., SHW2 in

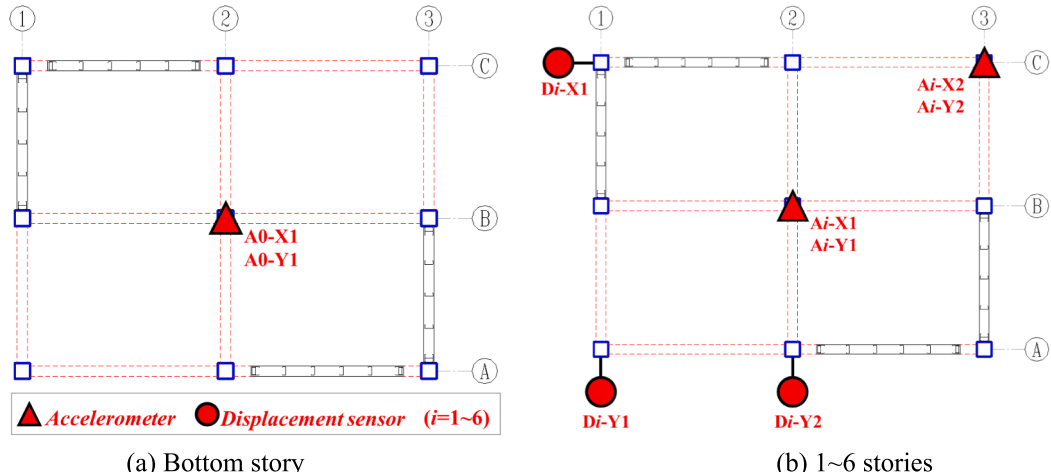


Fig. 11. Arrangement of acceleration and displacement sensors.

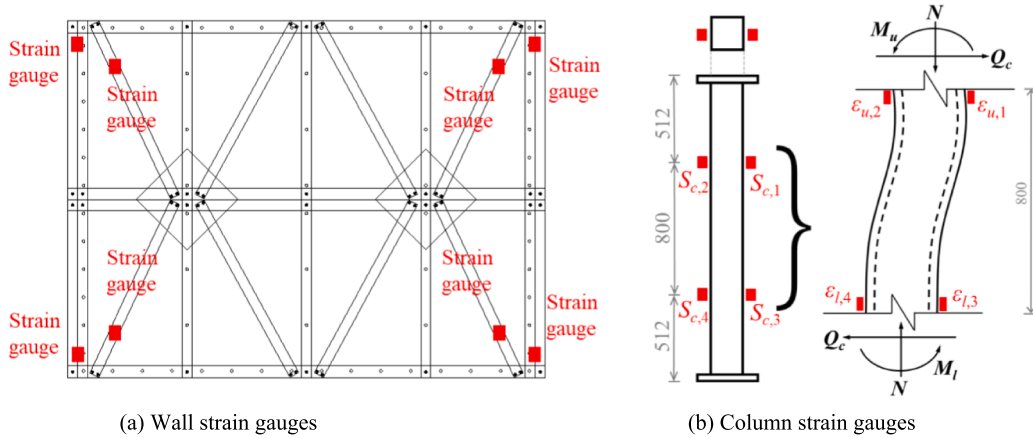


Fig. 12. Arrangement of strain gauges.

Code [48]). It was noted that all the ground motions were bidirectional. The test model was subjected to the seismic excitations with the designed precautionary intensity of 8-degree at three hazard levels (63%, 10% and 2 ~ 3% possibility of exceedance within 50 years). Moreover, the rare earthquake conditions corresponding to 8.5-degree intensity were included to test the structural collapse resistance. Firstly, the original records of the above-mentioned earthquakes were adjusted in amplitude to the code-specified PGA [38], as shown in Fig. 13. The tabulated errors compared to the design response spectrum at the unscaled fundamental period ( $T_1$ ) were also given, all within the specified tolerance of 20%. Then, the PGA ratio of the secondary component to the primary component of the bidirectional earthquakes should be 0.85. After that, to fulfill the similarity relationships, the seismic excitations were scaled in PGA and time according to the acceleration scale factor ( $S_a = 1.5$ ) and the time scale factor ( $S_t = 2/3$ ). Finally, white noise cases were added in the loading scheme as shown in Table 5.

#### 4. Test results and analyses

##### 4.1. Test phenomena

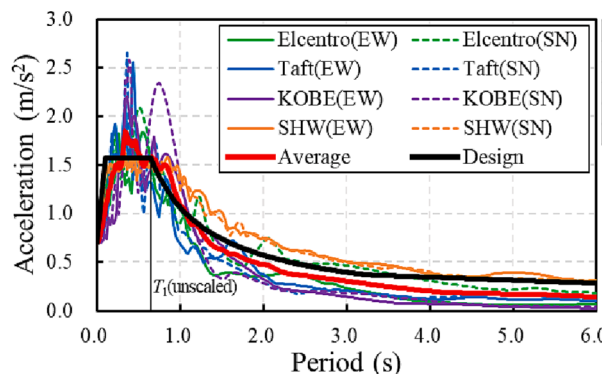
Table 6 lists the main test phenomena for the CFSF-FSWS test model. The deformation features of the structural components were observed during the shaking table tests (Fig. 14). When the PGA was 0.105 g (FOE8), the sounds of shear-wall sheathing sheets bulging and denting were heard. The structure was in elastic stage and no residual deformation was observed after each excitation. When the PGA reached 0.3 g (DBE8), the low-story shear-wall sheathing sheets were creased (Fig. 14a) and some of the corner screw holes were extruded and deformed (Fig. 14b). When the PGA reached 0.6 g (MCE8), the mid-story

shear-wall sheathing sheets also showed creases. Some corner screws of the low-story walls were pulled out (Fig. 14c). In addition, some concrete slabs had minor cracks at the corner of the reserved holes (Fig. 14d). When the PGA increased to 0.765 g (MCE8.5), the creases on the sheathing sheets were observed in almost all walls of the six stories. The creases were the most obvious in the low-story walls (Fig. 14e). More of the corner screws in the low-story walls fell off (Fig. 14f). However, the cracks in the concrete floor slabs did not expand. Throughout the tests, there was no failure of the bolted connections in the CFS frame, indicating that the bolts well ensured the frame performance (Fig. 14gh). The damage was mainly concentrated on sheathing sheets and sheathing-to-member screw connections of CFS framing shear walls, achieving the design objective of “separated gravity and lateral resisting systems”. And the frame beams did not yield and deform at the locations of the concentrated forces from hold-downs.

##### 4.2. Dynamic properties

###### 4.2.1. Fundamental period

After each seismic intensity level or vital loading cases, a white noise case was set to identify the structural dynamic properties. The transfer function was extracted from the input and output acceleration data. The corresponding natural frequency was then obtained by analyzing the peak of the real part curve of the transfer function. Fig. 15 illustrates the typical transfer function curves for obtaining natural frequencies. The natural frequencies and the fundamental periods were reciprocal to each other. Table 7 summarizes the X- and Y-directional natural frequencies and the fundamental periods (Fig. 16a) of the test model. It could be seen that the structural initial natural frequencies in the X- and Y-directions were both 2.25 Hz, corresponding to fundamental period of 0.444 s. The structural fundamental periods gradually increased with the increase of



	Elcentro(EW)	Taft(EW)	KOBE(EW)	SHW(EW)	Average
Acc(m/s²)	1.44	1.25	1.69	1.53	1.54
Ratio	93.1%	80.9%	109.0%	98.7%	99.3%
Elcentro(SN)					
Taft(SN)					
KOBE(SN)					
SHW(SN)					
Acc(m/s²)	1.42	1.65	1.84	1.48	
Ratio	91.5%	106.9%	118.9%	95.6%	

Fig. 13. Unscaled spectral acceleration of the ground motions.

**Table 5**

Loading scheme of the shaking table tests.

Sequence	Earthquake intensity	Ground motion	PGA(g) X	Y	Sequence	Earthquake intensity	Ground motion	PGA(g) X	Y
1	White Noise	WN1	0.050	0.050	23	MCE8	El. Centro	0.510	0.600
2	FOE8	El. Centro	0.105	0.089	24		WN6	0.050	0.050
3			0.089	0.105	25		TAFT	0.600	0.510
4		TAFT	0.105	0.089	26			0.510	0.600
5			0.089	0.105	27		WN7	0.050	0.050
6		Kobe	0.105	0.089	28		Kobe	0.600	0.510
7			0.089	0.105	29			0.510	0.600
8		Shanghai	0.105	0.089	30		WN8	0.050	0.050
9			0.089	0.105	31		Shanghai	0.600	0.510
10	White Noise	WN2	0.050	0.050	32		WN9	0.050	0.050
11	DBE8	El. Centro	0.300	0.255	33		Shanghai	0.510	0.600
12			0.255	0.300	34	White Noise	WN10	0.050	0.050
13		TAFT	0.300	0.255	35	MCE8.5	Kobe	0.765	0.650
14			0.255	0.300	36			0.650	0.765
15		Kobe	0.300	0.255	37		WN11	0.050	0.050
16			0.255	0.300	38		TAFT	0.765	0.650
17		Shanghai	0.300	0.255	39			0.650	0.765
18			0.255	0.300	40		WN12	0.050	0.050
19	White Noise	WN3	0.050	0.050	41		El. Centro	0.765	0.650
20	White Noise	WN4	0.050	0.050	42		WN13	0.050	0.050
21	MCE8	El. Centro	0.600	0.510	43		El. Centro	0.650	0.765
22		WN5	0.050	0.050	44	White Noise	WN14	0.050	0.050

**Table 6**  
Test phenomena.

Sequence	PGA (g)	Description of the test phenomena and observations
Cases 1–9	0.105	Noise of the steel sheet sheathing. No other obvious observations.
Cases 10–18	0.300	Creases appeared on the sheathing of low-story walls (Fig. 14a). Some corner self-drilling screw holes were extruded and deformed (Fig. 14b).
Cases 19–33	0.600	Creases appeared on the sheathing of low-story walls. Some corner self-drilling screws were pulled out (Fig. 14c). Cracks appeared on the concrete slabs (Fig. 14d).
Cases 34–44	0.765	Creases appeared on the sheathing of all walls and were severe on low-story walls (Fig. 14e). More self-drilling screws in the fell off (Fig. 14f). The CFS frame kept intact (Fig. 14gh).

the seismic intensity. Moreover, the natural frequencies in the X-direction were generally larger than those in the Y-direction after DBE8 seismic intensity, which indicated that the X-directional stiffness of the structure was relatively stronger and degraded more slowly. This was mainly due to the larger span of the test model in the X-direction, which owned better overturning resistance.

#### 4.2.2. Damping ratio

Damping ratio could effectively reflect the energy dissipation capacity of the structure. Through analyzing the transfer function curves by the half-power bandwidth method, the damping ratios of the structure were listed in Table 7 and shown in Fig. 16b. The initial damping ratio of the structure was 3.30% and 3.37% in the X- and Y-directions, respectively. With the increase of seismic intensity, the damping ratio gradually increased to the final maximum value 6.95% (Y-direction). This implied that the structural energy dissipation capacity increased

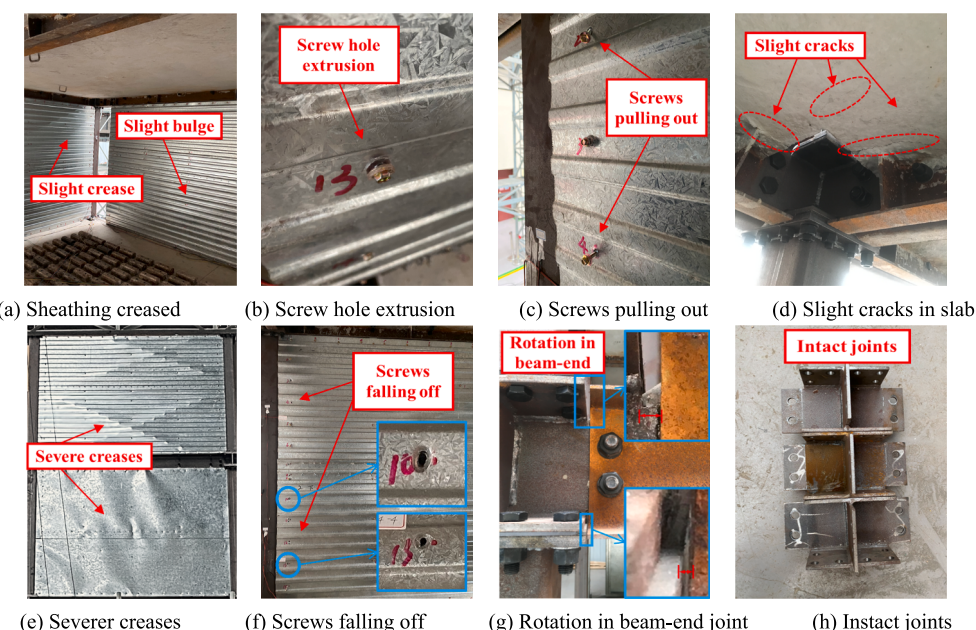


Fig. 14. Test observations.

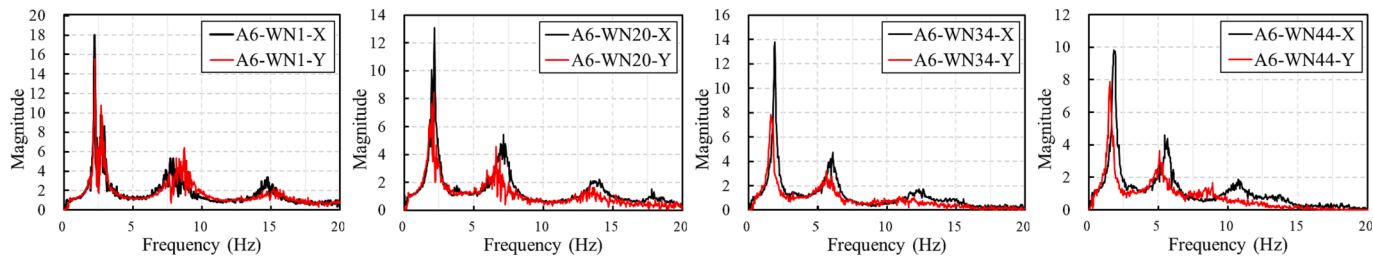


Fig. 15. Typical transfer function curves.

Table 7

Frequencies, periods and damping ratios of the test model.

White noise Sequence	X-direction Frequency (Hz)	Period (s)	Damping ratio	Y-direction Frequency (Hz)	Period (s)	Damping ratio
1	2.25	0.444	3.30%	2.25	0.444	3.37%
10	2.25	0.444	3.45%	2.25	0.444	3.41%
19	2.19	0.457	3.59%	2.13	0.471	3.45%
20	2.19	0.457	3.66%	2.13	0.471	3.72%
22	2.00	0.500	3.62%	1.88	0.533	4.11%
24	1.94	0.516	3.86%	1.84	0.542	4.40%
27	1.91	0.525	4.22%	1.84	0.545	4.90%
30	1.91	0.527	3.96%	1.84	0.549	5.18%
32	1.88	0.533	4.41%	1.75	0.571	5.43%
34	1.88	0.536	4.68%	1.63	0.615	5.63%
37	1.88	0.541	4.89%	1.63	0.620	5.84%
40	1.88	0.544	5.43%	1.63	0.623	6.03%
42	1.88	0.548	5.70%	1.56	0.640	6.64%
44	1.75	0.571	6.22%	1.50	0.667	6.95%

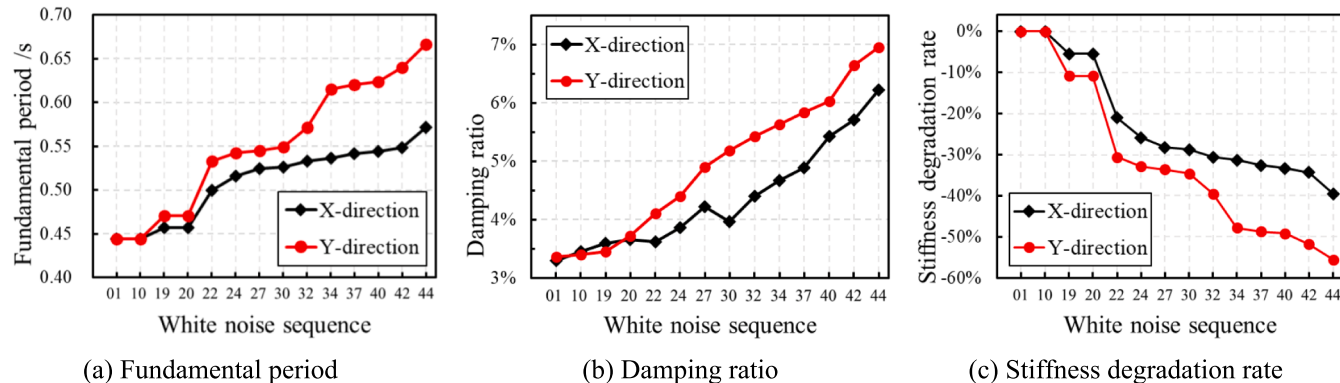


Fig. 16. Variations of structural fundamental period, damping ratio and stiffness degradation rate.

with the accumulation of damage. The X-directional damping ratios were generally smaller than Y-directional damping ratios, which showed that the Y-directional walls suffered more damage due to the relatively weaker stiffness. It was also found that the structural damping ratios tended to increase in a stepwise manner with the increases of seismic intensities, i.e., from frequent to medium to rare earthquakes. The mean values of damping ratios for FOE8, DBE8, MCE8 and MCE8.5 were 3.38%, 3.61%, 4.53% and 5.96%, respectively, which could guide the definition of damping ratios for different seismic intensities in subsequent finite element simulations. Moreover, zigzag jitter appeared in the local curve, which was mainly due to the pulling and dropping of the screws in the CFS walls during the consecutive seismic excitations. The loss of the frictional resistance in the original screw connection positions led to the decrease of the damping ratio in the structure.

#### 4.2.3. Stiffness degradation

The changes in the stiffness of a structure could be reflected by the changes in the natural frequencies. According to the knowledge of

structural dynamics, for an equivalent single-degree-of-freedom system, the structural stiffness was proportional to the square of the natural frequency. Therefore, the stiffness degradation rate coefficient  $\lambda_{SDR}$  of the structure was defined in Eq. (3).

$$\lambda_{SDR} = \frac{k_i - k_0}{k_0} = \frac{f_i^2 - f_0^2}{f_0^2} \quad (3)$$

where  $k_0$  and  $f_0$  were the initial stiffness and natural frequency of the structure, respectively;  $k_i$  and  $f_i$  were the structural stiffness and natural frequency corresponding to  $i_{th}$  white noise case.

The relationship between the  $\lambda_{SDR}$  and the white noise cases is shown in Fig. 16c. It showed that the stiffness of the structure gradually degraded as the seismic intensity increased, which was mainly due to the damage accumulation of the lateral resistant components (CFS walls). From the appearing of creases on the sheathing sheets and extrusion of screw holes during medium earthquakes, and then to the falling off of self-tapping screws during rare earthquakes, the structural stiffness was

weakened. The diaphragm effect of the sheathing of the CFS walls gradually decreased. The stiffness degradation trends of the test model in two directions were not consistent. The stiffness degradation in the Y-direction was greater than that in the X-direction. This also indicated that the Y-direction of the structure was the weak stiffness direction. Eventually, the Y-directional stiffness decreased more than 60% from the initial stiffness. The walls were severely damaged, but the CFS frame did not show significant damage, and the test model showed no danger of collapse. The structural system showed good seismic performance.

#### 4.3. Seismic responses

##### 4.3.1. Acceleration responses

The accelerations corresponding to each story of the test model were measured by the arranged bidirectional accelerometers. To facilitate the comparison of acceleration responses from different types and intensities of seismic inputs, the acceleration amplification factor ( $\beta$ ) was defined, which was the absolute ratio of story acceleration to shaking table acceleration, as defined by Eq. (4).

$$\beta = |a_i/a_0| \quad (4)$$

where  $a_0$  was the acceleration of the shaking table and  $a_i$  was the acceleration of the  $i$ th story.

The envelope curves of  $\beta$  corresponding to all loading cases were classified according to the mainshock direction, intensity, and earthquakes, as presented in Fig. 17. In general, the  $\beta$  increased with the increase of the structure heights. The CFS framing shear walls, which played a major role in lateral resistance, were different in configurations for each story. The wall stiffnesses decreased from the first story to sixth story, which made the envelope curves of  $\beta$  exhibit the S-shape. The distribution characteristics of the  $\beta$  envelope curves for different earthquakes were different, which was mainly related to the spectral characteristics of different earthquakes and the damage in the structure. From the comparison of different intensities, it could be seen that the  $\beta$  corresponding to FOE8 and DBE8 cases in the same direction were generally larger than those in MCE8 and MCE8.5 cases. This was due to the fact that the structure basically kept elastic working condition in FOE8 and DBE8 cases, while some components entered plasticity in MCE8 and MCE8.5 cases. The effect of acceleration amplification was thus weakened. It was noted that the bidirectional seismic inputs were

the X- and Y- directional components of the same earthquake, with differences in the spectral characteristics. The acceleration amplification factors in different directions presented different features. In general, the magnitude and dispersion in the Y direction were greater.

##### 4.3.2. Displacement responses

The displacement responses of the test model were measured by means of the arranged cable-type displacement sensors. The relative displacements of each story were then obtained by subtracting the displacements of adjacent floors. The relative displacements were finally divided by the story height to obtain the inter-story drift ratio (IDR). The IDR envelope curves along the structural heights are plotted in Fig. 18. It could be seen that under the action of FOE8 earthquakes, the maximum IDRs of the structure in the X- and Y- directions were 0.16% and 0.18%, respectively; under the action of DBE8 earthquakes, the maximum IDRs increased to 0.50% and 0.57% in X- and Y- directions; and in MCE8 earthquakes the maximum IDRs increased to 0.82% and 1.21% in X- and Y- directions; finally under the MCE8.5 earthquakes, the maximum IDRs in the X- and Y- directions reached up to 1.08% and 1.53%, respectively. It should be noted that according to the similarity relationship in Table 1, the scale factor of rotation angle was 1.0 ( $S_\phi = 1.0$ ). Therefore, it was concluded that the above IDR values under different intensity earthquakes satisfied the required limits for elastic inter-story displacement angle of 1/250 [38,49] and elastic-plastic inter-story displacement angle of 1/50 [38] for multi-story and high-rise steel structures.

In general, the peak IDRs of the structure increased with the increase of seismic intensity. The peak IDRs corresponding to El-Centro and Shanghai waves were generally larger than those of Taft and Kobe waves. Although the seismic inputs in X- and Y- directions were two components of the same earthquake, the comparison of IDR curves showed that: when the intensity was low (FOE8, DBE8), the IDRs in X-direction were just slightly lower than those in Y-direction; when the intensity increased to MCE8, the IDRs in Y-direction were significantly larger; when the intensity increased to MCE8.5, the differences in IDRs between the two directions enlarged further. This also proved that the X-directional stiffness of the structure was greater. In the cases of low intensity earthquakes (FOE8, DBE8), the maximum IDRs along the structural height basically appeared at the second or third story. This was mainly due to the higher inter-story shear forces at the lower stories,

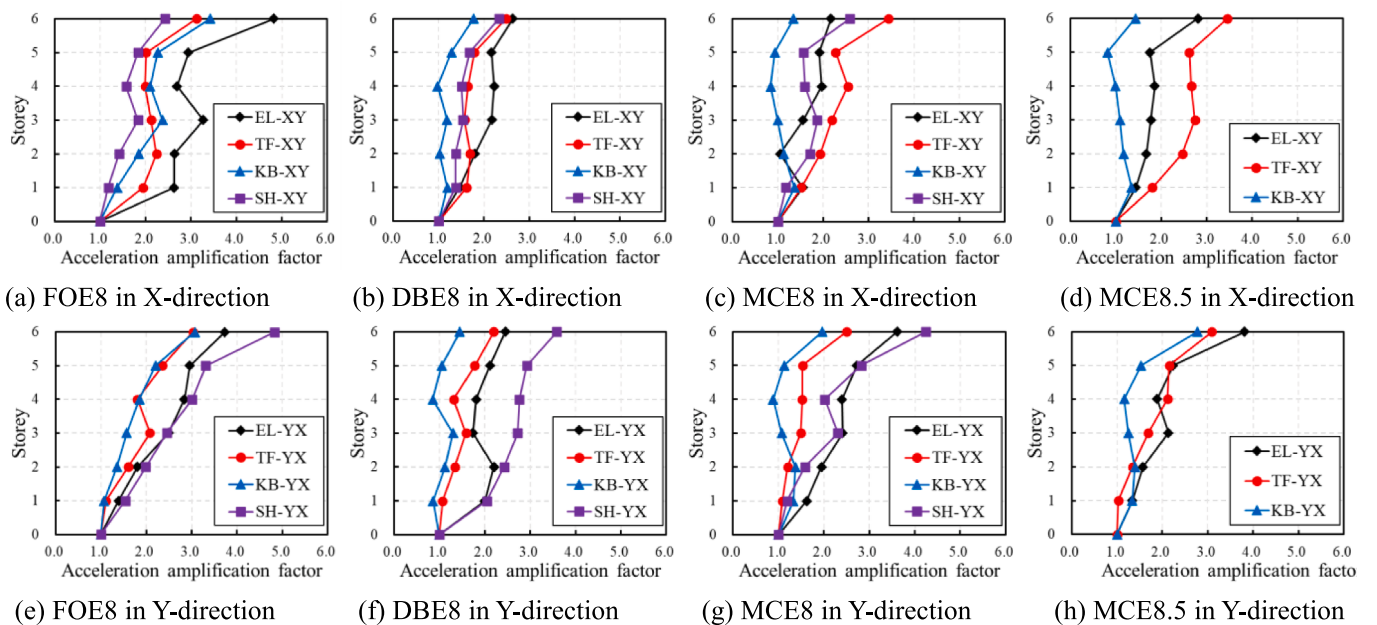


Fig. 17. Envelope curves of acceleration amplification factor  $\beta$ .

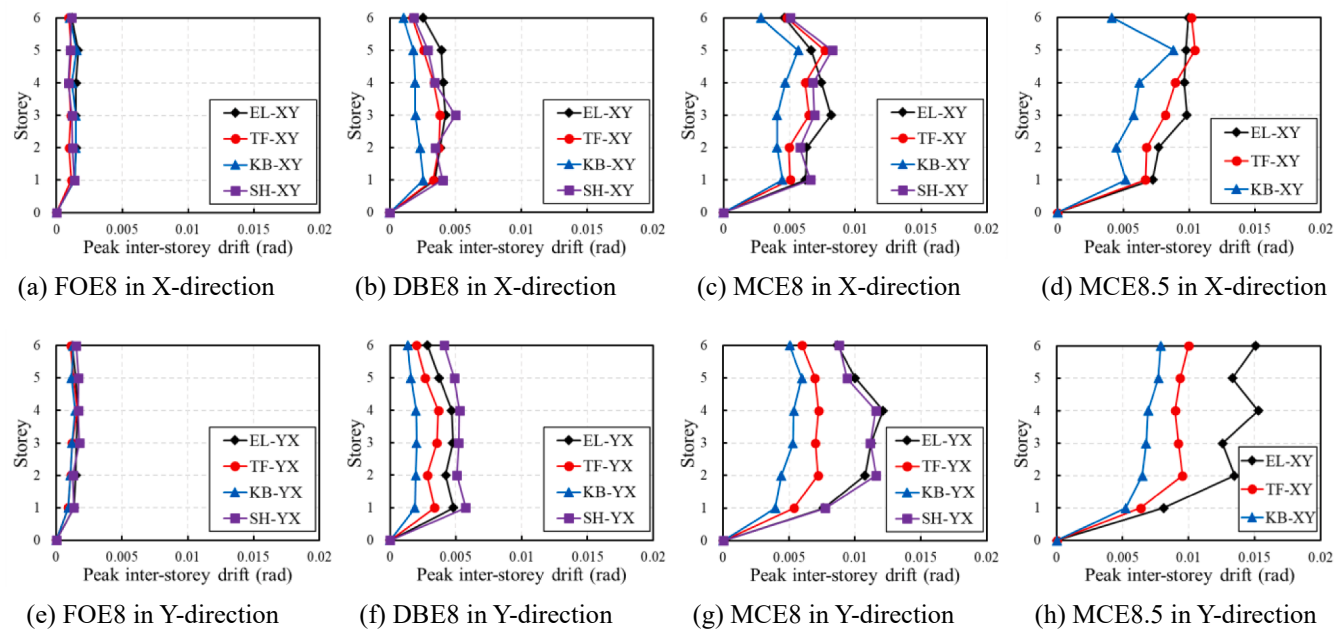


Fig. 18. Envelope curves of inter-story drift ratio IDR.

as well as the near-rigid connection of the bases. In addition, under high intensity earthquakes (MCE8, MCE8.5), the maximum IDRs tended to appear at the higher stories, reflecting the characteristics of bending deformation.

The peak roof drift ratios (PRDRs) of the test model for all loading cases are obtained and plotted in Fig. 19a. The PRDR was defined as the peak ratio of the roof displacement relative to the foundation to the height of the structure. It could be seen that the PRDRs responses generally increased with seismic intensities. And the PRDRs of the structure were generally greater in the Y-direction than in the X-direction, due to the smaller span and weaker anti-overturning capacity in Y-direction. Another vital displacement response index was the diaphragm responses. The schematic diagram of the maximum diaphragm deflection (MDD) and the results for the long side of all loading cases are shown in Fig. 19b. It could be seen that the MDDs were all in a very small magnitude, due to the concrete slabs used and the reliable connections for the slabs at each story. According to ASCE 7 [50], the diaphragm flexibility could be evaluated using the MDD/ADVE ratio as illustrated in Fig. 19b. When the MDD/ADVE ratio exceeded 2.0, the diaphragm was considered to be flexible. In fact, the maximum MDD/ADVE ratio for the test model was only 0.142. Therefore, the diaphragms could all be considered rigid in the plane.

#### 4.3.3. Strain responses

The strain responses of the CFS framing shear walls were measured and analyzed. The strain gauges were arranged at critical locations of the CFS wall skeletons where plastic deformations were likely to occur (chord studs or truss braces). The maximal strain values of all wall strain gauges for different intensities were extracted and plotted in Fig. 20. The

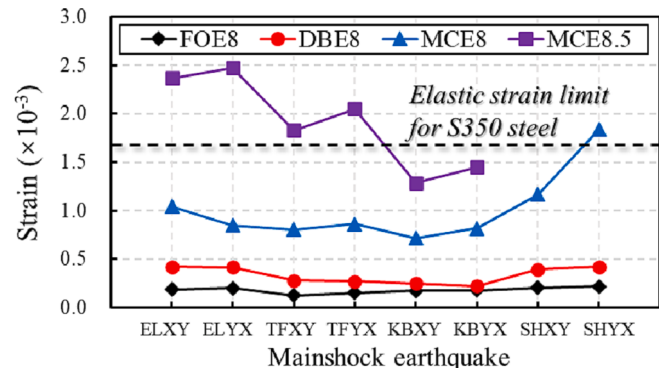


Fig. 20. Maximal wall strain values for different intensities.

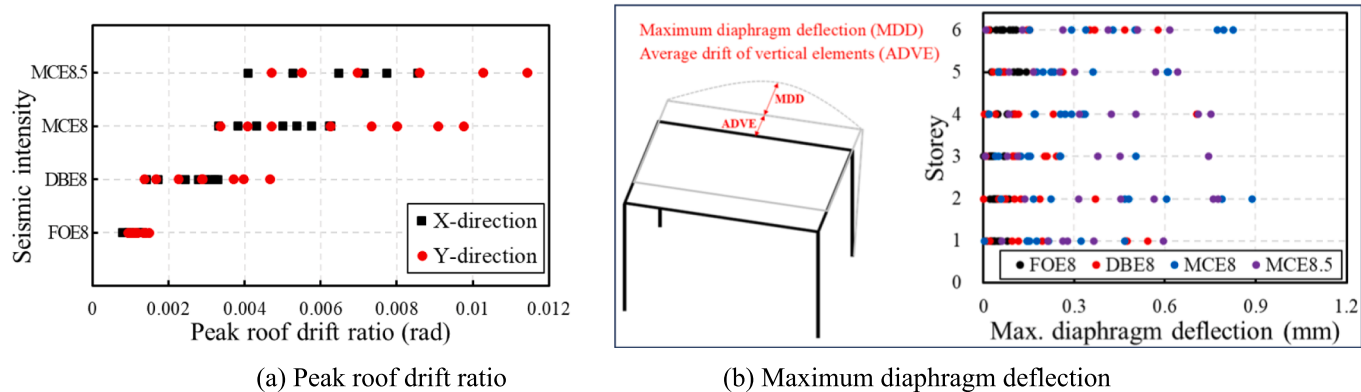


Fig. 19. Other important displacement response indicators.

wall strains increased with the increase of seismic intensity. Under both FOE8 and DBE8 intensities, the wall strains were at a very low elastic level ( $<0.5 \times 10^{-3}$ ); while under the action of MCE8 earthquakes, especially the Shanghai artificial waves, the wall strains increased sharply and even exceeded the nominal yield strain of S350 steel ( $1.7 \times 10^{-3}$ ); and in MCE8.5 cases, the wall strains all maintained at a high level, with the strains generated by the El-Centro earthquake being the largest. The above analysis showed that the wall skeletons basically remained elastic under FOE8 and DBE8 earthquakes; while under MCE8 and MCE8.5 earthquakes, the larger inter-story shear forces and deformations made some chord studs yielded and participated in plastic energy dissipation.

#### 4.3.4. Load sharing between frame and walls

With Eqs. (1) to (2), the structural inter-story shear forces and the shear forces carried by the frame columns could be calculated for each story. To quantify the contribution of CFS frame to the lateral force resisting, the  $R_{\text{frame}}$  factor was defined to evaluate the proportion of inter-story shear forces carried by the CFS frame at each story. For  $k^{\text{th}}$  story, the corresponding  $R_{\text{frame}}$  could be calculated from Eq (5):

$$R_{\text{frame}} = |Q_{c,k}^{\text{peak}} / Q_k^{\text{peak}}| \times 100\% \quad (5)$$

where  $Q_k^{\text{peak}}$  was the peak inter-story shear forces (positive or negative) at  $k^{\text{th}}$  story;  $Q_{c,k}^{\text{peak}}$  was the corresponding shear forces carried by frame columns at  $k^{\text{th}}$  story.

Taking the Loading Case 25 as an example, the X-directional inter-story and CFS frame shear forces time-history curves for the second and third story of the test model are exhibited in Fig. 21. For the second story (Fig. 21a), the peak inter-story shear force was 238.97 kN and the CFS frame bore 47.91 kN force under the MCE8 Taft earthquake. Thus, the  $R_{\text{frame}}$  of the second story was 20.0% in this case. Similarly, the  $R_{\text{frame}}$  of the third story for Loading Case 25 was calculated to be 24.1% as illustrated in Fig. 21b.

The  $R_{\text{frame}}$  factors of the second and third stories in the X-direction for all loading cases were shown in Fig. 22. It could be seen from Fig. 22a that for the second story of the structure, the  $R_{\text{frame}}$  ranged from 7.1% to 13.1% for FOE8 earthquakes, from 12.2% to 20.9% for DBE8 earthquakes, from 18.4% to 27.0% for MCE8 earthquakes, and from 26.8% to 30.7% for MCE8.5 earthquakes. The  $R_{\text{frame}}$  increased with the increase of seismic intensity. This was due to the fact that the steel frame basically remained elastic and the accumulated damage in the CFS framing shear walls led to the decreases in wall stiffness and force sharing. The Fig. 22b showed the  $R_{\text{frame}}$  of the third story. Since the third-story CFS walls were weaker than the second-story walls, the corresponding  $R_{\text{frame}}$  were generally larger than those of the second story under the same intensity earthquakes, with the maximum  $R_{\text{frame}}$  value reaching 32.8% in the MCE 8.5 earthquakes. The other features in the  $R_{\text{frame}}$  of the two stories were similar. Generally speaking, most of the inter-story shear

forces in the CFSF-FSWS were borne by the CFS framing shear walls. Meanwhile, the wall stiffness decreased with increasing earthquake-induced inter-story shear forces, thus resulting the CFS frame which basically remained elastic, to bear more shear forces.

## 5. Discussions

In the present study, we achieved the first six-story shaking table tests of CFSF-FSWS which combined CFS framing shear walls and CFS frame. And the design concept of “separated gravity and lateral resisting systems” was realized by suitable joints and connections design. The main failure modes during the tests were the accumulation damages of the CFS framing shear walls. The CFS frame was instinct and basically maintained elastic working condition. The structure exhibited favorable seismic performance in terms of structural responses. The findings of this study could promote the application of CFS structures in multi-story and even mid-rise buildings. However, due to the lab conditions, a 2:3 scaling ratio was selected and the number of stories was limited to six. And earthquakes above 9-degree were not considered. Moreover, the CFS framing shear walls in each story of the test model were arranged in the same way. A full-scale test model with higher height, higher earthquake intensity, and more flexible wall arrangements would be more conducive to investigate the feasibility of applying the CFSF-FSWS to multi-story and mid-rise buildings. This was one of the directions for future efforts.

## 6. Conclusions

In this paper, the seismic performance of a six-story floor-by-floor assembled CFSF-FSWS was studied by large-scale shaking table tests. The structural dynamic property, seismic response and damage mechanism were analyzed. Based on the results of the study, the following conclusions were drawn:

- (1) The damage of the multi-story CFSF-FSWS under seismic actions was characterized by screw connection failure and sheathing failure in CFS framing shear walls. Under FOE8 earthquakes, the structure remained elastic; with the increase of seismic intensity especially after MCE8, the shear-wall sheathing sheets presented creases, and the screw connections were damaged to failure. The diaphragm effect of shear-wall sheathing was gradually weakened. There was no obvious damage in the CFS frame.
- (2) With the increase of PGA, the structural frequency and stiffness decreased and the damping ratio increased. The creasing of CFS wall sheathing and pulling-out of screw connections were the key factors affecting the dynamic properties. The prefabricated concrete floor slab had slight cracks, but did not expand in subsequent loading, ensuring the stiffness of the floor and roof.

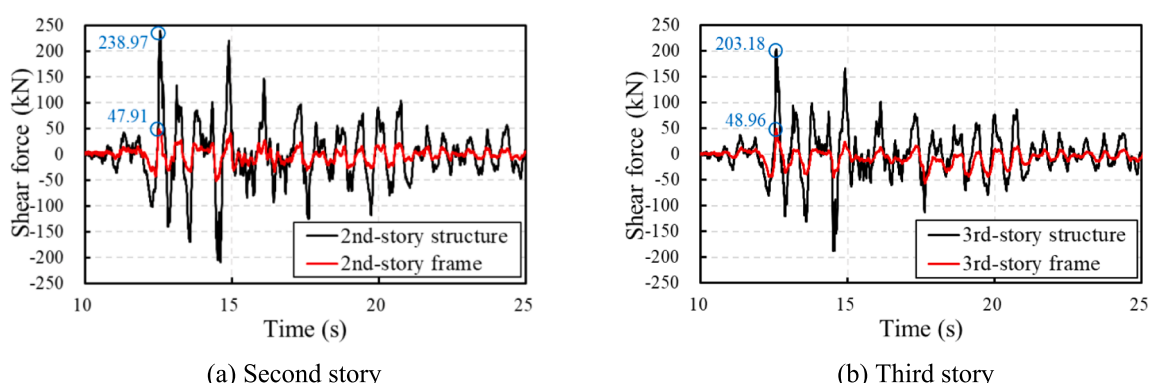


Fig. 21. Inter-story and CFS frame shear forces in Loading Case 25.

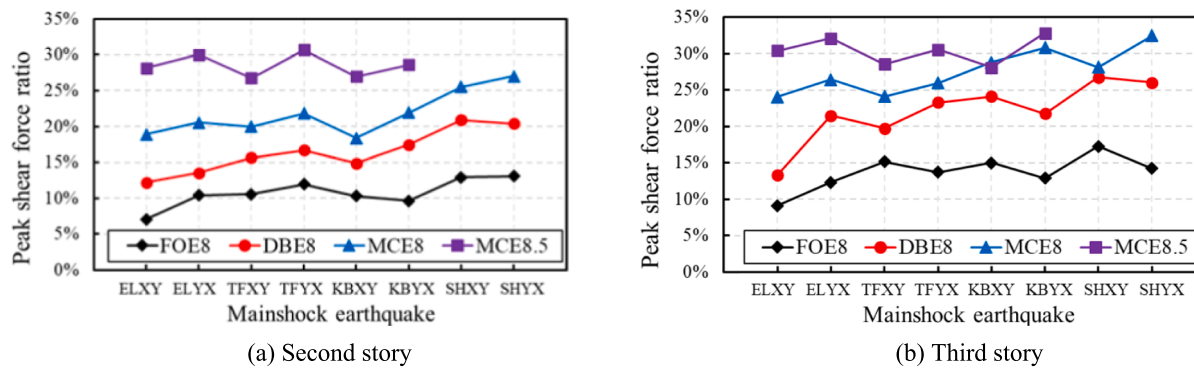


Fig. 22. Peak inter-story shear force shearing ratio of CFS frame.

- (3) In 2nd and 3rd stories, the CFS frame peak shear force ratios  $R_{\text{frame}}$  were below 25% in DBE8 earthquakes; the peak value of  $R_{\text{frame}}$  was 32.8% (MCE8.5). The CFS frame stably bore vertical loads and did not change the lateral-resisting mode of the structural system. The lateral resistances from CFS framing shear walls were always predominated. However, the percentage of shear resistance provided by CFS framing shear walls decreased due to the stiffness degradation caused by accumulated damage.
- (4) With the proper design of joints, slabs and connections, the CFSF-FSWS exhibited favorable assemblability. The design concept of “separated gravity and lateral resisting systems” was successfully implemented. The CFS frame system basically remained elastic during the tests and stably carried the vertical load, while the damage was concentrated on the CFS framing shear wall system.
- (5) Unlike the shear deformation of the conventional CFS framing wall structure, the inter-story displacement responses of CFSF-FSWS were S-shape at the late loading stage. The structure presented a certain degree of bending deformation characteristics.
- (6) The proposed CFSF-FSWS system achieved the desired seismic performance. The structural peak IDRs under frequent, medium and rare earthquakes were within the code limit and met the requirements of multi-level seismic prevention, by which the effectiveness of the new structural system was established.

#### CRediT authorship contribution statement

**Fu-Wei Wu:** Investigation, Resources, Software, Visualization, Validation, Data curation, Writing – original draft, Formal analysis.  
**Yuan-Qi Li:** Conceptualization, Methodology, Funding acquisition, Supervision, Project administration, Writing – review & editing.

#### Declaration of Competing Interest

The authors declare that they have no known competing financial interests or personal relationships that could have appeared to influence the work reported in this paper.

#### Data availability

The authors do not have permission to share data.

#### Acknowledgements

The authors gratefully acknowledge the financial supports from the National Natural Science Foundation of China (Grant No. 51538002 and No. 51978500).

#### References

- [1] Zhang W, Mandavian M, Yu C. Lateral strength and deflection of cold-formed steel shear walls using corrugated sheathing. *J Constr Steel Res* 2018;148:399–408. <https://doi.org/10.1016/j.jcsr.2018.06.009>.
- [2] Zhang W, Yu C, Mahdavian M. Seismic Performance of Cold-Formed Steel Shear Walls Using Corrugated Sheathing with Slits. *J Struct Eng* 2019;145:04019014. [https://doi.org/10.1061/\(ASCE\)ST.1943-541X.0002284](https://doi.org/10.1061/(ASCE)ST.1943-541X.0002284).
- [3] Zhang W, Mahdavian M, Yu C. Different slit configuration in corrugated sheathing of cold-formed steel shear wall. *J Constr Steel Res* 2018;150:430–41. <https://doi.org/10.1016/j.jcsr.2018.08.035>.
- [4] Yu C, Tian Y, Yan W, Zhang W. Novel energy dissipation bracing designed for corrugated sheet-sheathed cold-formed steel shear wall. *J Struct Eng* 2021;147:04021171. [https://doi.org/10.1061/\(ASCE\)ST.1943-541X.0003147](https://doi.org/10.1061/(ASCE)ST.1943-541X.0003147).
- [5] Shi Y, Ran X, Xiao W, Ke K, Xiang Y, Deng R. Experimental and numerical study of the seismic behavior of cold-formed steel walls with diagonal braces. *Thin-Walled Struct* 2021;159:107318. <https://doi.org/10.1016/j.tws.2020.107318>.
- [6] Tian H-W, Li Y-Q, Yu C. Testing of steel sheathed cold-formed steel trussed shear walls. *Thin-Walled Struct* 2015;94:280–92. <https://doi.org/10.1016/j.tws.2015.04.009>.
- [7] Wu F-W, Li Y-Q. Multi-level simulation studies on seismic performance evaluation of steel-sheathed cold-formed steel framing shear walls. *Journal of Building Engineering* 2022;61:105302. <https://doi.org/10.1016/j.jobe.2022.105302>.
- [8] Briere V, Santos V, Rogers CA. Cold-formed steel centre-sheathed (mid-ply) shear walls. *Soil Dyn Earthq Eng* 2018;114:253–66. <https://doi.org/10.1016/j.soildyn.2018.07.008>.
- [9] Torabian S, Schafer BW. Cyclic experiments on sidelap and structural connectors in steel deck diaphragms. *J Struct Eng* 2021;147:04021028. [https://doi.org/10.1061/\(ASCE\)ST.1943-541X.0002981](https://doi.org/10.1061/(ASCE)ST.1943-541X.0002981).
- [10] Shi Y, Luo Z, Xu Y, Zou Y, Xu L, Ma Q. Experimental study on the seismic behavior of high-performance cold-formed steel plate shear walls. *Eng Struct* 2022;251:113552. <https://doi.org/10.1016/j.engstruct.2021.113552>.
- [11] Liu B, Hao J-P, Zhong W-H, Wang H. Performance of cold-formed-steel-framed shear walls sprayed with lightweight mortar under reversed cyclic loading. *Thin-Walled Struct* 2016;98:312–31. <https://doi.org/10.1016/j.tws.2015.09.024>.
- [12] Wang W, Wang J, Guo L, Liu Y, Zhang R. Cyclic performance tests and numerical analysis of prefabricated CFS shear walls filled with lightweight EPS mortars. *Eng Struct* 2021;243:112554. <https://doi.org/10.1016/j.engstruct.2021.112554>.
- [13] Wu H, Chao S, Zhou T, Liu X. Cold-formed steel framing walls with infilled lightweight FGD gypsum Part I: Cyclic loading tests. *Thin-Walled Struct* 2018;132:759–70. <https://doi.org/10.1016/j.tws.2018.04.003>.
- [14] Wu H, Sui L, Wang J, Zhou T. Cycle performance tests and numerical modeling of infilled CFS shear walls. *J Constr Steel Res* 2020;168:106010. <https://doi.org/10.1016/j.jcsr.2020.106010>.
- [15] Chen Z, Mohammed A, Du Y, Mashrahi WAH, Zhao B, Huang J. Experimental and numerical study on seismic performance of square and L-shaped Concrete-filled steel tubes column Frame-Buckling steel plate shear walls. *Eng Struct* 2023;274:115155. <https://doi.org/10.1016/j.engstruct.2022.115155>.
- [16] Jiang Z-Q, Yan T, Zhang A-L, Su L, Shen C-J. Experimental research on special steel frame with stiffened double steel plate shear wall. *J Constr Steel Res* 2022;189:107067. <https://doi.org/10.1016/j.jcsr.2021.107067>.
- [17] Wang X, Ye J. Reversed cyclic performance of cold-formed steel shear walls with reinforced end studs. *J Constr Steel Res* 2015;113:28–42. <https://doi.org/10.1016/j.jcsr.2015.05.012>.
- [18] Wang X, Ye J. Cyclic testing of two- and three-story CFS shear-walls with reinforced end studs. *J Constr Steel Res* 2016;121:13–28. <https://doi.org/10.1016/j.jcsr.2015.12.028>.
- [19] Tian H-W, Li Y-Q, Zhou Y. Theoretical analysis and testing of steel frame with cold-formed steel shear walls with steel sheathing. *J Struct Eng* 2018;144:04018079. [https://doi.org/10.1061/\(ASCE\)ST.1943-541X.0002057](https://doi.org/10.1061/(ASCE)ST.1943-541X.0002057).
- [20] Mortazavi M, Sharifi P, Ronagh H, Samali B, Kildashti K. Lateral behaviour of hybrid cold-formed and hot-rolled steel wall systems: Experimental investigation. *J Constr Steel Res* 2018;147:422–32. <https://doi.org/10.1016/j.jcsr.2018.04.035>.

- [21] Usefi N, Ronagh H, Sharafi P. Lateral performance of a new hybrid CFS shear wall panel for mid-rise construction. *J Constr Steel Res* 2020;168:106000. <https://doi.org/10.1016/j.jcsr.2020.106000>.
- [22] Gad EF, Duffield CF, Hutchinson GL, Mansell DS, Stark G. Lateral performance of cold-formed steel-framed domestic structures. *Eng Struct* 1999;21:83–95. [https://doi.org/10.1016/S0141-0296\(97\)90129-2](https://doi.org/10.1016/S0141-0296(97)90129-2).
- [23] Kim T-W, Wilcoski J, Foutch DA, Lee MS. Shaketable tests of a cold-formed steel shear panel. *Eng Struct* 2006;28:1462–70. <https://doi.org/10.1016/j.engstruct.2006.01.014>.
- [24] Li Y, Shen Z, Yao X, Ma R, Liu F. Experimental investigation and design method research on low-rise cold-formed thin-walled steel framing buildings. *J Struct Eng* 2013;139:818–36. <https://doi.org/10.1016/ASCE.JST.1943-541X.0000720>.
- [25] Peterman KD, Stehman MJJ, Madsen RL, Buonopane SG, Nakata N, Schafer BW. Experimental seismic response of a full-scale cold-formed steel-framed building. II: Subsystem-level response. *J Struct Eng*. 2016;142:04016128. <https://doi.org/10.1016/ASCE.JST.1943-541X.0001578>.
- [26] Schafer BW, Ayhan D, Leng J, Liu P, Padilla-Llano D, Peterman KD, et al. Seismic Response and Engineering of Cold-formed Steel Framed Buildings. *Structures* 2016; 8:197–212. <https://doi.org/10.1016/j.istruc.2016.05.009>.
- [27] Peterman KD, Stehman MJJ, Madsen RL, Buonopane SG, Nakata N, Schafer BW. Experimental seismic response of a full-scale cold-formed steel-framed building. I: System-level response. *J Struct Eng*. 2016;142:04016127. <https://doi.org/10.1016/ASCE.JST.1943-541X.0001577>.
- [28] Fiorino L, Macillo V, Landolfo R. Shake table tests of a full-scale two-story sheathing-braced cold-formed steel building. *Eng Struct* 2017;151:633–47. <https://doi.org/10.1016/j.istruc.2017.08.056>.
- [29] Fiorino L, Bucciero B, Landolfo R. Shake table tests of three storey cold-formed steel structures with strap-braced walls. *Bull Earthquake Eng* 2019;17:4217–45. <https://doi.org/10.1007/s10518-019-00642-z>.
- [30] Zhao Y, Yu C, Zhang W, Xie Z, Yu S, Du X. Shake table tests of a corrugated steel sheathed cold-formed steel structure. *Journal of Building Engineering* 2022;60: 105161. <https://doi.org/10.1016/j.jobe.2022.105161>.
- [31] Wang X, Pantoli E, Hutchinson TC, Restrepo JI, Wood RL, Hoehler MS, et al. Seismic performance of cold-formed steel wall systems in a full-scale building. *J Struct Eng* 2015;141:04015014. <https://doi.org/10.1016/ASCE.JST.1943-541X.0001245>.
- [32] Hutchinson TC, Wang X, Hegemier G, Kamath P, Meacham B. Earthquake and postearthquake fire testing of a midrise cold-formed steel-framed building. I: building response and physical damage. *J Struct Eng* 2021;147:04021125. <https://doi.org/10.1016/ASCE.JST.1943-541X.0003097>.
- [33] Wang X, Hutchinson TC. Earthquake and postearthquake fire testing of a midrise cold-formed steel-framed building. II: shear wall behavior and design implications. *J Struct Eng* 2021;147:04021126. <https://doi.org/10.1016/ASCE.JST.1943-541X.0003098>.
- [34] Ye J, Jiang L. Simplified analytical model and shaking table test validation for seismic analysis of mid-rise cold-formed steel composite shear wall building. *Sustainability* 2018;10:3188. <https://doi.org/10.3390/su10093188>.
- [35] Jiang L, Zhang X, Ye J, Jiang L, Zhou L. Seismic behavior and damage assessment of mid-rise cold-formed steel-framed buildings with normal and reinforced beam-column joints. *Archiv Civ Mech Eng* 2021;21:125. <https://doi.org/10.1007/s43452-021-00278-4>.
- [36] Zhou X, Yao X, Xu L, Shi Y, Ke K, Liu L. Shake table tests on a full-scale six-storey cold-formed thin-walled steel-steel plate shear wall structure. *Thin-Walled Struct* 2022;181:110009. <https://doi.org/10.1016/j.tws.2022.110009>.
- [37] Li Y-Q, Wu F-W, Tan M-Q. Static performance of non-through one-side bolted end-plate joint for floor-by-floor assembled steel structures. *Structures* 2023;48: 288–303. <https://doi.org/10.1016/j.istruc.2022.12.083>.
- [38] Ministry of Housing and Urban-Rural Development of the People's Republic of China. GB 50011-2010 Code for seismic design of buildings. Beijing, China: Architecture & Building Press; 2010. (in Chinese).
- [39] Kenan H, Azeloglu O. Design of scaled down model of a tower crane mast by using similitude theory. *Eng Struct* 2020;220:110985. <https://doi.org/10.1016/j.istruc.2020.110985>.
- [40] Yang J, Lu Z, Li P. Large-scale shaking table test on tall buildings with viscous dampers considering pile-soil-structure interaction. *Eng Struct* 2020;220:110960. <https://doi.org/10.1016/j.istruc.2020.110960>.
- [41] Ministry of Construction of the People's Republic of China. GB 50017-2017 Standard for design of steel structures. Beijing, China: China Planning Press; 2017. (in Chinese).
- [42] American Iron and Steel Institute. S100-16 North American Specification for the Design of Cold-Formed Steel Structural Members. Washington, DC: AISI; 2016.
- [43] American Iron and Steel Institute. S400-15 North American Standard for Seismic Design of Cold-Formed Steel Structural Systems. Washington, DC: AISI; 2015.
- [44] Ministry of Housing and Urban-Rural Development of the People's Republic of China. GB 50009-2012 Load code for the design of building structures. Beijing, China: Architecture & Building Press; 2012. (in Chinese).
- [45] Zhang A, Xie Z, Zhang Y, Lin H. Shaking table test of a prefabricated steel frame structure with all-bolted connections. *Eng Struct* 2021;248:113273. <https://doi.org/10.1016/j.istruc.2021.113273>.
- [46] He M, Luo Q, Li Z, Dong H, Li M. Seismic performance evaluation of timber-steel hybrid structure through large-scale shaking table tests. *Eng Struct* 2018;175: 483–500. <https://doi.org/10.1016/j.istruc.2018.08.029>.
- [47] He M, Li Z, Lam F, Ma R, Ma Z. Experimental investigation on lateral performance of timber-steel hybrid shear wall systems. *J Struct Eng* 2014;140:04014029. <https://doi.org/10.1016/ASCE.JST.1943-541X.0000855>.
- [48] Construction and Transportation Commission of Shanghai. DGJ08-9-2013 Code for seismic design of buildings. Beijing, China: Architecture & Building Press; 2013. (in Chinese).
- [49] Ministry of Housing and Urban-Rural Development. JGJ/T 421-2018 Technical Standard for Cold-Formed Thin-Walled Steel Multi-Storey Residential Buildings. Beijing, China: Architecture & Building Press; 2018. (in Chinese).
- [50] American Society of Civil Engineers. ASCE 7-16 Minimum Design Loads for Buildings and Other Structures. Virginia, USA: ASCE/SEI; 2016.